Computed Ligand Effects on the Oxidative Addition of Phenyl Halides to Phosphine Supported Palladium(0) Catalysts

Claire L. McMullin, Natalie Fey and Jeremy N. Harvey

Supporting Information[1]

Table of Contents

[1] Note that an additional ESI file, containing xyz coordinates for all optimised geometries, is also available.

SI1. Computational Details

a. Methodology

Unless stated otherwise, structures were optimized in the Gaussian 03 and Gaussian 09 packages (see section SI1b for full citations), with the B3LYP density functional.[1] The standard 6-31G(d) basis set was used, but with only the five spherical harmonic components of the polarization functions, for all H, C, P and Cl atoms.[2] For Br, Pd and I, the corresponding Stuttgart relativistic ECPs[3] were used to describe the core 28, 28 and 46 electrons, respectively, together with their associated triple zeta basis[3] as implemented in Gaussian. Additional polarization functions were added, with one f function for Pd (exponent 1.1484[4]), and one d function each for Br and I (exponent 0.45 and 0.4, respectively). This basis set combination is denoted as BS1.

Frequencies were calculated with B3LYP/BS1, and were used to assess the nature of stationary points, to compute zero-point energies, and to derive gas-phase statistical mechanics values for the thermal and entropic corrections at the temperatures as indicated. The statistical mechanics calculations use the simple rigid-rotor harmonic oscillator approximation. Computed entropies in particular are very sensitive to numerical error in the values of the lowest-frequency modes, so these were inspected visually for all species. Soft torsional modes with frequencies lower than 30 cm^{-1} were found for most species, though values lower than 7 cm^{-1} were rarely obtained. Tests in which frequencies were computed again after re-optimization with tighter geometry convergence criteria did not lead to material changes in frequencies, so we estimate that the numerical error in the reported Gibbs energy terms due to incomplete geometry convergence is less than 1 kcal mol^{-1}.

Solvation Gibbs energies were obtained from single point calculations on the B3LYP/BS1 geometries with the Integral Equation Formalism Polarizable Continuum Model (IEF-PCM) continuum dielectric solvation model,[5] using toluene (ε=2.379, probe radius = 2.757) as the solvent.

Additional single point energy calculations used the B3LYP/BS1 optimized geometries to obtain improved energy values with a larger basis set. This basis set comprised the same core potential for Pd, Br and I as in BS1, but with larger aug-cc-pVTZ treatment of the valence electrons.[4,6] For H, C, P and Cl, the 6-311+G* all-electron basis was used. [7] This combination is denoted as BS2 throughout.

Note that the computed Gibbs energies within Gaussian use standard conditions corresponding to an ideal gas at a pressure of 1 atm at the corresponding temperature. These were converted to yield Gibbs energies with a solution phase standard state of 1 mol dm^{-3}. This was performed by adding to each species' free energy as computed in Gaussian, at the relevant temperature, a free-energy correction term equal to RT ln(V_molar_gas / V_molar_solution). In this equation, R is the gas constant, T is the absolute temperature, V_molar_gas is the volume occupied by one mole of ideal gas

at the temperature considered, and V_molar_solution is the volume occupied by one mole of species in a standard solution of concentration 1 mole dm^{-3}, *i.e.i.e.* 1 dm^3.[8]

A final correction term was based on single-point energy calculations using the dispersion–corrected B3LYP-D functional[9] as implemented in the Orca program[10] (corresponding to the B3LYP-D2 version). For these calculations, the VDZ_P basis set as implemented in ORCA was used, and was found to give similar energetics (not shown here) to BS1. However, the B3LYP-D calculations were used merely to provide a correction term $\Delta E_{disp,B3LYP\text{-}D}$ = E(B3LYP-D/VDZ_P) – E(B3LYP/VDZ_P).

Calculations of the seven PCy_3 conformers as free ligand and coordinated to [AuCl] and $[PdCl_3]^-$ metal fragments (discussed in section SI2a) were computed using the Jaguar program (v6.0).[11] The B3LYP hybrid density functional[1f 1a-e,12] was employed with the Jaguar triple-ζ form of the standard Los Alamos ECP basis set (LACV3P) used on the Au and Pd transition metal atoms, and the 6-31G* basis for all other atoms. This has been denoted as BSJ1.

The *tetrakis* PPh_3 structure $\mathbf{12_{Ph}}$ was taken from a crystal structure in the Cambridge Structural Database[13] (ref. code TTPPDB)[14] whilst the $[Pd(PCy_3)_3]$ complex ($\mathbf{11_{Cy}}$) was optimized from a molecular mechanics GMMX conformer search using the MMX forcefield as implemented in PCModel.[15] For the SPhos calculations, crystal structures MAKBIK[16] and MAKBEG[16] were used to build the $Pd(SPhos)_2$ geometries (ac and cc respectively) and the *chloro* dimeric structure JIMMEY[17] used as the basis for geometry *s*-$\mathbf{10_{SP}}$. Conformers for some of the other complexes of PCy3 and SPhos were also explored with GMMX conformer searches using the MMX forcefield as implemented in PCModel,[15] but lower energy conformers were not found.

B3LYP-D2/BS1 geometry optimisations discussed in the ESI have used G09 rev. B1 with the keyword iop(3/124=3). For some of the very hindered complexes, convergence could not be achieved with standard settings and looser convergence criteria (opt=loose) were employed in those cases. Section SI4b also includes results for optimisation with the BP86 functional, [1a,18] again using BS1 as described above.

The effects of different types of dispersion correction to B3LYP (-D2, -D3 and D3-BJ) as shown in Section SI4e have been computed with Grimme's DFT-D3 programme, available at http://www.thch.uni-bonn.de/tc/index.php?section=downloads&subsection=getd3&lang=english[19]

b. Full Gaussian References

Gaussian 03, Revision C.02, M.J. Frisch, G.W. Trucks, H.B. Schlegel, G.E. Scuseria, M.A. Robb, J.R. Cheeseman, J. Montgomery, J. A., T. Vreven, K.N. Kudin, J.C. Burant, J.M. Millam, S.S. Iyengar, J. Tomasi, V. Barone, B. Mennucci, M. Cossi, G. Scalmani, N. Rega, G.A. Petersson, H. Nakatsuji, M.

Hada, M. Ehara, K. Toyota, R. Fukuda, J. Hasegawa, M. Ishida, T. Nakajima, Y. Honda, O. Kitao, H. Nakai, M. Klene, X. Li, J.E. Knox, H.P. Hratchian, J.B. Cross, V. Bakken, C. Adamo, J. Jaramillo, R. Gomperts, R.E. Stratmann, O. Yazyev, A.J. Austin, R. Cammi, C. Pomelli, J.W. Ochterski, P.Y. Ayala, K. Morokuma, G.A. Voth, P. Salvador, J.J. Dannenberg, V.G. Zakrzewski, S. Dapprich, A.D. Daniels, M.C. Strain, O. Farkas, D.K. Malick, A.D. Rabuck, K. Raghavachari, J.B. Foresman, J.V. Ortiz, Q. Cui, A.G. Baboul, S. Clifford, J. Cioslowski, B.B. Stefanov, G. Liu, A. Liashenko, P. Piskorz, I. Komaromi, R.L. Martin, D.J. Fox, T. Keith, M.A. Al-Laham, C.Y. Peng, A. Nanayakkara, M. Challacombe, P.M.W. Gill, B. Johnson, W. Chen, M.W. Wong, C. Gonzalez, J.A. Pople, Wallingford CT **2004**.

Gaussian 09, Revision B.01, M. J. Frisch, G. W. Trucks, H. B. Schlegel, G. E. Scuseria, M. A. Robb, J. R. Cheeseman, G. Scalmani, V. Barone, B. Mennucci, G. A. Petersson, H. Nakatsuji, M. Caricato, X. Li, H. P. Hratchian, A. F. Izmaylov, J. Bloino, G. Zheng, J. L. Sonnenberg, M. Hada, M. Ehara, K. Toyota, R. Fukuda, J. Hasegawa, M. Ishida, T. Nakajima, Y. Honda, O. Kitao, H. Nakai, T. Vreven, J. A. Montgomery, Jr., J. E. Peralta, F. Ogliaro, M. Bearpark, J. J. Heyd, E. Brothers, K. N. Kudin, V. N. Staroverov, T. Keith, R. Kobayashi, J. Normand, K. Raghavachari, A. Rendell, J. C. Burant, S. S. Iyengar, J. Tomasi, M. Cossi, N. Rega, J. M. Millam, M. Klene, J. E. Knox, J. B. Cross, V. Bakken, C. Adamo, J. Jaramillo, R. Gomperts, R. E. Stratmann, O. Yazyev, A. J. Austin, R. Cammi, C. Pomelli, J. W. Ochterski, R. L. Martin, K. Morokuma, V. G. Zakrzewski, G. A. Voth, P. Salvador, J. J. Dannenberg, S. Dapprich, A. D. Daniels, O. Farkas, J. B. Foresman, J. V. Ortiz, J. Cioslowski, and D. J. Fox, Gaussian, Inc., Wallingford CT **2010**.

SI2. Conformers

The issue of phosphine ligand conformational change has been explored for P^iPr_3, which generally shows similar conformational preferences to PCy_3, in a recent study by Maseras, Lledós and co-workers.[20] Previous studies in the structural chemistry group at Bristol[21] have used the Cambridge Structural Database (CSD)[13] as a source of conformers of P-donor ligands in different coordination environments. The results discussed here explore the seven possible PCy_3 conformers observed crystallographically in 865 *X*-ray structures, as well as studying the crystal structures of SPhos available in the CSD (2010 version 5.31).

a. PCy_3

The ligand PCy_3 is more demanding to model than other symmetrical phosphines, such as PH_3, PPh_3 and P^tBu_3, as the three cyclohexyl substituents can adopt a number of different orientations; in addition, their motion is correlated and, depending on coordination environment, interconversion can be difficult. This leads to a number of energetically distinct conformers with varying steric profiles when coordinated in organometallic complexes. Therefore, the steric profile of the ligand is non-uniform, and computational study of this ligand requires careful thought and consideration to ensure that the correct conformer is being calculated. The orientation of the cyclohexyl ring relative to the phosphorus donor atom and metal fragment (Z) is defined by the torsion angle Z-P-C_1-H (τ_n), as shown in Figure SI2a, specified by the position of the hydrogen on the P bound carbon atom (C_1).

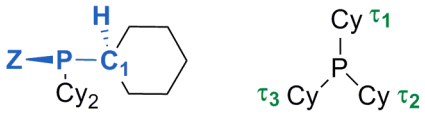

Figure SI2a PCy_3 conformation defining torsion Z-P-C_1-H (τ_n)

Rotation of the cyclohexyl groups about the P—C bond leads to interconversion of the conformers. The hydrogen on C_1 can adopt three distinct orientations. When it is *trans* to the metal fragment ($\tau \sim 180$ °) this is classified as *anti* (*a*), while at $\tau \sim \pm 60$ ° the orientation is described as *gauche*, with the torsion value either positive (g^+) or negative (g^-).

The structure correlation model introduced by Bürgi and Dunitz[22] classifies unpopulated regions of conformational space as high in energy on the potential energy hypersurface; this model can be used to interpret ligand conformer populations. Populated regions of conformational space are energetically accessible, with heavily populated clusters identified as conformational minima. To compare the crystallographic literature consistently, the coordination environment of the ligand should be the same. While there is no specific reason to expect energies of given conformers of the complexes to correspond to the inverse of the number of times they are observed in the CSD,[21b], it seems likely that

the most commonly observed conformations are more likely to be energetically accessible. Here computational study allows the direct comparison of different ligand conformers, allowing to set these data mining results into context.

The CSD was thus mined for crystal structures of PCy_3 ligands complexed to transition metal centres. A total of 865 structures were identified, giving 1363 individual entries. A symmetrical phosphorus donor ligand, with all three substituents the same (PA_3) such as PCy_3, has C_{3v} symmetry. Application of the six symmetry operators of this point group generates different torsion combinations, listed in Table SI2a, and must be applied to the data extracted from the CSD. Once the data has been symmetry expanded, the related *a*, g^+ or g^- identifiers are assigned to each cyclohexyl τ value. From the 27 conformations available (3^3), these are reduced to seven unique conformer classes **A**—**G**, listed in Table SI2b and shown in Figure SI2b.

Table SI2a Symmetry operators applied to torsions τ_1, τ_2 and τ_3 for a C_{3v} symmetric phosphine ligand

Operator	**τ_1**	**τ_2**	**τ_3**
E	τ_1	τ_2	τ_3
C_3^1	τ_3	τ_2	τ_1
C_3^2	τ_2	τ_3	τ_1
σ	—τ_1	—τ_3	—τ_2
σ + C_3^1	—τ_3	—τ_2	—τ_1
σ + C_3^2	—τ_2	—τ_1	—τ_3

Table SI2b The seven unique conformers and additional symmetry related conformations

Conformer		**Equivalent conformation**	**Ideal Symmetry**
A	*aaa*		C_{3v}
B	$g^+g^+g^+$	$g^+g^+g^+$	C_3
C	g^+g^+a	g^+ag^+, ag^+g^+, g^-g^-a, g^-ag^-, ag^-g^-	C_1
D	g^+aa	ag^+a, aag^+, g^-aa, ag^-a, aag^-	C_1
E	g^+g^-a	g^-ag^+, ag^+g	C_s
F	g^-g^+a	g^+ag^-, ag^-g^+	C_s
G	$g^-g^+g^+$	$g^+g^+g^-$, $g^+g^-g^+$, $g^+g^-g^-$, $g^-g^-g^+$, $g^-g^+g^-$	C_1

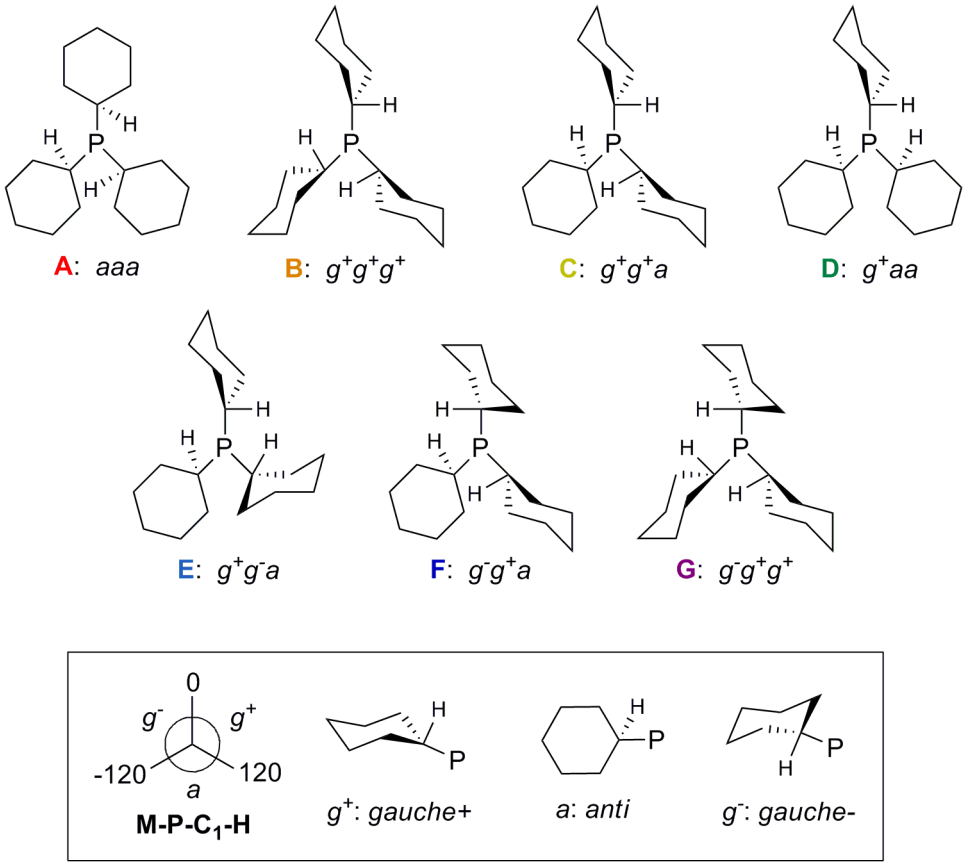

Figure SI2b The seven PCy_3 conformers looking down the M—P bond and their defined M-P-C_1-H torsions

The most prevalent conformer is **F**, g^-g^+a, with over 60 % of the PCy_3 ligands captured by the CSD as this conformer (see Figure SI2c). The second most common conformer is **C**, g^+g^+a, which is also the conformation of the two non-complexed PCy_3 crystal structures in the CSD. Conformers **A**, **B**, **E** and **G** are not represented well and constitute only 2.2 % of the structures found, with the final conformer **D** representing 5.5 % of the population, implying that these five conformers are less favoured for PCy_3.

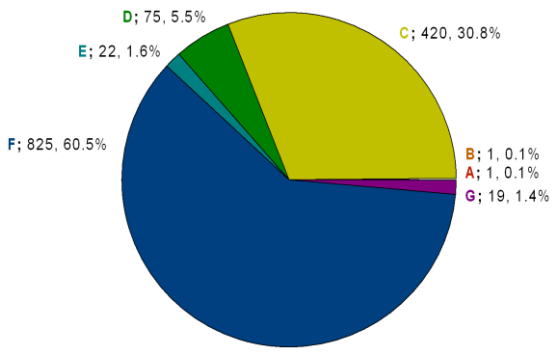

Figure SI2c CSD conformer population for PCy_3

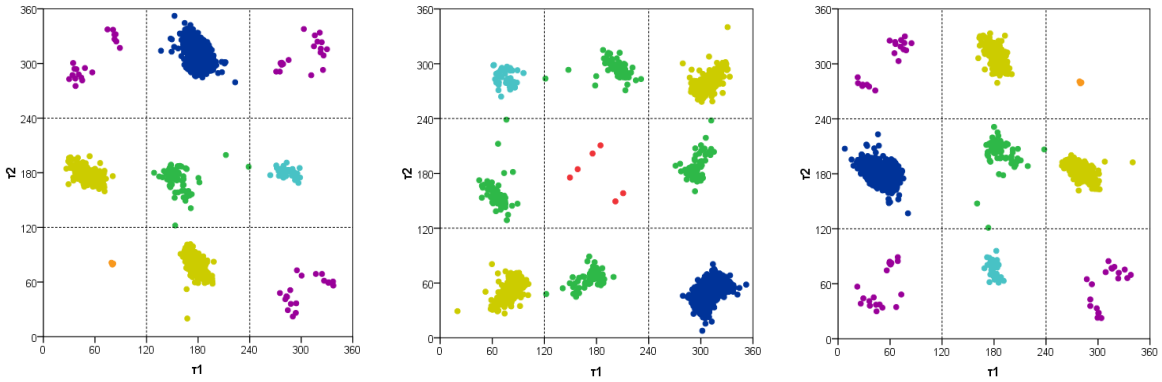

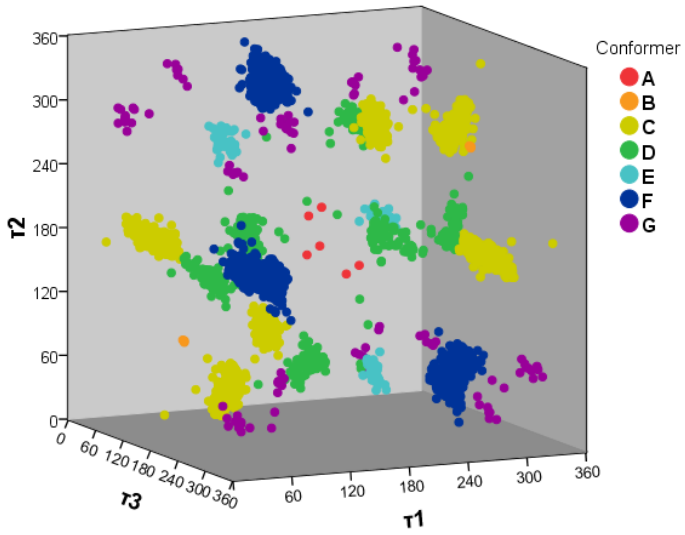

Figure SI2d Conformer plots for PCy_3; 2D plots of τ_1 versus τ_2 for $\tau_3 = g^+$, *a* and g^-, and a combined 3D plot

Conformers have been plotted with respect to the three torsions, τ_n, in Figure SI2d. As the substituents of PCy_3 are well-defined cyclohexyl rings, there are no obvious interconversion pathways between conformers in these plots, suggesting that these are likely to be high energy processes. Clusters of conformers are observed in regions of three-dimensional space, suggesting that individual conformers correspond to well-defined minima, with the exception of a few conformer **D** structures, which lie close to the conformation classification boundary (*i.e.i.e.* where τ ~ 120 or 240 °). This, added to the knowledge that **D** borders the two most prevalent conformers **F** and **C**, suggests that structures containing a **D** PCy_3 conformer may instead be in transition from one conformer to another. Observation of conformer **D** may be a result of rapid crystallization before the preferred free phosphine conformation (**C**) has been able to convert to conformer, **F**, which appears to be more stable on complexation.

Extending this idea further, metal complexes where the PCy_3 conformation is **C** (g^+g^+a) could also arise

from rapid cooling and crystallisation of the sample, whilst the majority of structures with conformer **F** are slowly formed after interconversion to the thermodynamically favoured conformer when complexed. Inspection of the structures suggests that both conformers **C** and **F** strike a good balance between minimising unfavourable intra- and inter-ligand contacts. The remaining conformers are most likely a result of unusual metal environments (overcrowded metal centres or those with very low coordination numbers, unusual metal clusters or co-ligands) or crystal packing, forcing less energetically favoured PCy_3 conformers.

Previous studies from the Orpen group observed conformer preferences were influenced by several factors;[21b] intra-ligand, inter-ligand and anomeric effects, illustrated in Figure SI2d. The former effect refers to close *syn* contacts between *aa* and g^+g^- substituents, which are present in conformers **A**, **D**, **E** and **G**. Inter-ligand effects describe *cis* ligands (L) favouring the phosphorus donor ligand to have reduced bulk with fewer *gauche* substituent conformations, as in **A** and **D**. This effect is lessened in lower coordinate complexes which allow the ligand to adopt conformers with substituents in *gauche* orientations, increasing the steric profile. Anomeric effects, which are not relevant here, refer to the delocalisation of a phosphorus lone pair into an O—C σ* orbital, favouring at least one *anti* conformation in phosphites.

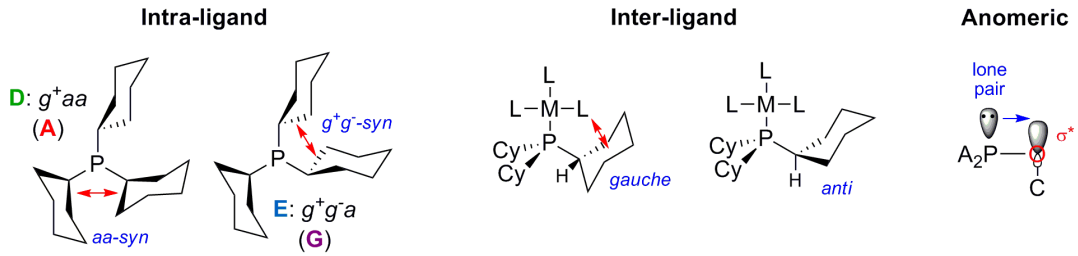

Figure SI2d Summary of effects that influence ligand conformer preference.

To understand the energetic preference for individual conformers in different coordination environments, simple DFT calculations (see section SI1a for details) were carried out for the pro-ligand PCy_3, a linear gold(I) complex $[AuCl(PCy_3)]$ and a square-planar palladium(II) complex $[PdCl_3(PCy_3)]^-$; the results are shown in Table SI2c. There are three different orientations for docking the different PCy_3 ligand conformers to the square-planar palladium complex. The docking torsion (τ_{Cl} shown in Figure SI2e) describes which cyclohexyl group the *cis* chloride is aligned with so that Cl_{cis}-Pd-P-C_1 ~ 0 °.

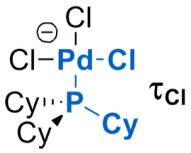

Figure SI2e The docking torsion τ_{Cl}, describing which τ_n of PCy_3 is aligned to a *cis* chloride of the

$[PdCl_3(PCy_3)]^-$ fragment

Table SI2c Relative energies (B3LYP/BSJ1) in kcal mol^{-1} for the seven PCy_3 conformers in different coordination environments

	τ_{Cl}	**A** *aaa*	**B** $g^+g^+g^+$	**C** g^+g^+a	**D** g^+aa	**E** g^+g^-a	**F** g^-g^+a	**G** $g^-g^+g^+$
PCy_3		2.4	3.8	**0.0**	1.3	2.0	0.6	4.0
$[AuCl(PCy_3)]$		2.7	2.5	**0.0**	1.1	1.6	1.2	3.7
$[PdCl_3(PCy_3)]^-$	τ_1	10.0	[a]	[b]	0.6	1.1	**0.1**	4.1
	τ_2	10.1	[a]	3.3	0.6	1.2	**0.0**	9.9
	τ_3	10.0	[a]	[b]	0.6	2.7	**0.0**	4.1

[a] optimized to conformer **C**

[b] optimized to conformer **D**

For the uncomplexed ligand and linear gold complex the order of relative conformer energies is as follows:

C < **F** < **D** < **E** < **A** < **B** ~ **G.** This agrees with the conformer population distribution of crystal structures mined from the CSD, where the two examples of the free phosphine PCy_3 adopted conformer **C**, with the energetically next higher conformers **F** and **D** also highly populated in the database. However, the average coordination environment in the CSD for PCy_3 is more crowded than these model complex geometries and these results are not representative of all the data harvested from the CSD.

Indeed, a change in conformer energy preference can be observed when the ligand is bound to the four-coordinate square-planar palladium complex, giving **F** < **D** < **E** < **C** < **G** < **A** < **B.** Despite aligning the PCy_3 conformers so a *cis* chloride was in the plane of only one cyclohexyl group (τ_{Cl}), during optimization rotation about the Pd—P bond occurred, resulting in the same alignment of the *cis* chlorides to the PCy_3 ligand given for each τ_1, τ_2 and τ_3 orientation. Only one of the docked **C** conformers optimized to the desired conformation, the other two showed rotation of a *gauche*$^+$ Cy substituent, converting it to an *anti* position and hence conformer **D**. The same issue occurred for conformer **B** with the helically chiral C_3 conformer (ggg) undergoing rotation of one of the *gauche*$^+$ cyclohexyl groups to be *anti* and therefore becoming conformer **C**.

Based on the results of this conformer study, the two most popular low energy conformers, **F** and **C**, were chosen to investigate how conformer choice influences the reaction potential energy surface, extending our investigation into ligand effects. Computed Gibbs energies for the oxidative addition of phenyl bromide to PCy_3 ligated catalyst are given in Table SI2d. The values are calculated relative to the lowest energy conformer of $[Pd(PCy_3)_2]$, which is **F** (g^-g^+a). Dissociation of a ligand to form the

monoligated complex [Pd(PCy_3)] retains the same conformer preference, with **F** lower in energy than **C**; the optimised geometries are shown in Figure SI2f. With decreasing stability of the [Pd(PCy_3)] species, the Pd—P bond length marginally increases, with a Pd—P distance of 2.229 Å calculated for **F**, increasing to 2.234 Å for conformer **C**.

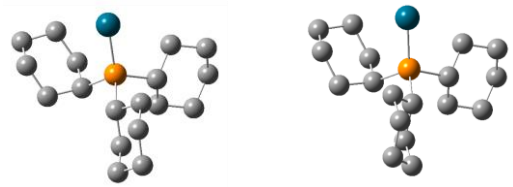

F *g⁻g⁺a*

C *g⁺g⁺a*

Figure SI2f Optimized geometries of the monoligated [Pd(PCy_3)] species for conformer **F** and **C**

In the monoligated structure [Pd(PCy_3)] for conformer **C** the *anti* cyclohexyl ring has 'risen' such that the end of the ring (carbon C_4) is in close proximity to the palladium metal centre (see Figure SI2f). In fact C_4 is 1.3 Å closer to palladium than in the equivalent structure for conformer **F**, and the Pd–P–C_4 angle has decreased from 98 ° to 76 °, suggesting a agostic interactions with a distance of 2.7 Å between hydrogens on carbons C_3 and C_5 and the palladium atom. These agostic interactions will stabilize the monoligated species, and other low-coordinate intermediates such as the T-shaped oxidative addition product, [Pd(Ph)(Br)(PCy_3)], although it is worth bearing in mind that this interaction might be dampened by solvation. In addition, this monoligated complex may not occur in isolation, coordinating solvent molecules instead.[23]

Table SI2d B3LYP-D2/BS2 Gibbs energies in kcal mol^{-1} for the oxidative addition of PhBr to [Pd(PCy_3)$_n$] for conformers **F** and **C** of PCy_3

	$\Delta G°$ (90 °C) + ΔG_{solv}	**F** *g⁻g⁺a*	**C** *g⁺g⁺a*
	L = PCy_3	0.0	1.1
1$_{Cy}$	[PdL]	18.5	21.8
2$_{Cy}$	[PdL$_2$]	0.0	0.2
3$_{Cy}$	[Pd(PhBr)L]	14.0	17.0
4$_{Cy}^{‡}$	[Pd(Ph···Br)L]‡	22.7	23.8
5$_{Cy}$	[Pd(Ph)(Br)L]	-9.3	-7.9
6$_{Cy}^{‡}$	[Pd(PhBr)L$_2$]‡	28.6	[a]

[a] not calculated for this conformer

These calculations, using the "best method" as described in section SI1a above (B3LYP-D2/BS2, $\Delta G°$ at 90 °C + ΔG_{solv}) and summarised in Table SI2d, suggest that complexes with ligands in conformer **F**

will give the lowest energy intermediates. However, this does not necessarily imply that this is the active catalyst in solution, as conformer interconversion may occur, especially as conformer **C** is thermodynamically preferred for the free ligand and ligand dissociation may be a low energy process. At this level of theory, conformer **F** is 1.1 kcal mol^{-1} lower in Gibbs energy than conformer **C**, while the bisligated intermediate [PdL_2] for conformer **C** is only 0.2 kcal mol^{-1} higher in Gibbs energy than the **F** equivalent complex, giving almost the same Gibbs energy for two different ligand conformerations with differing steric profiles in the same coordination environment. This implies that both **F** and **C** are low energy conformers for this linear structure. However, for complexes with higher coordination numbers, a clear preference for conformer **F** is shown and the results reported here refer to this conformer.

b. SPhos

Larger monophosphines with what might be called *pseudo*-hemi-labile characteristics, such as SPhos, complicate ligand dissociation further, as the flexible biaryl substituent can rotate about the P—C bond,[24] to favour lower complexes with lower coordination numbers. This flexibility is thought to prevent catalyst aggregation and decomposition, both prior to oxidative addition and after reductive elimination, suggesting that the ligand conformation is variable throughout the catalytic cycle, protecting and supporting the palladium centre when required.[24-25]

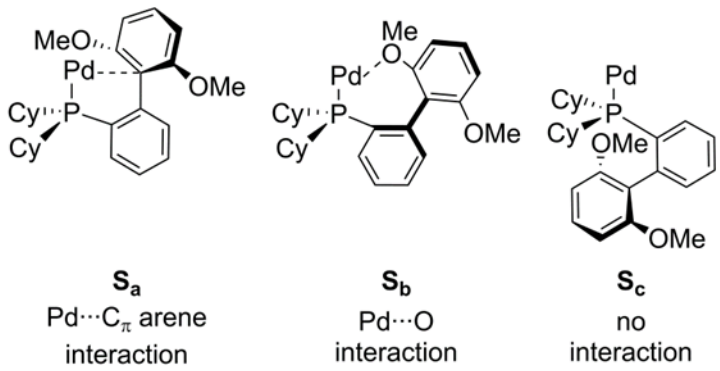

Scheme SI2a Three conformations of SPhos; $PCy_2(2\text{-}C_6H_4\text{-}2',6'\text{-}OMe\text{-}C_6H_3)$

We found a total of 21 complexes of SPhos in the CSD[26] (as of October 2012), 12 containing Pd, 5 Au, 3 Ir and one Cu complex. Three distinct conformations were identified; $\mathbf{S_a}$, $\mathbf{S_b}$ and $\mathbf{S_c}$ (see Scheme SI2a). In complexes with low coordination numbers (*i.e.*, 2 or 3 coordinate complexes) the biaryl substituent forms stabilizing Pd···C_π ($\mathbf{S_a}$; Pd-P-C-C ≈ 0 - 5°)[27] or Pd···O ($\mathbf{S_b}$; Pd-P-C-C ≈ 54°)[17] interactions. For higher-coordinate structures the biaryl group 'tucks' itself under the phosphorus atom and cyclohexyl groups, thereby reducing the steric bulk of the phosphine ligand ($\mathbf{S_c}$; Pd-P-C-C ≈ 140 - 160°).[16]

Ignoring the orientation of the biaryl substituent of the SPhos ligand and considering only the two cyclohexyl substituents, the ligand has C_s symmetry. The symmetry expansion of the clockwise Pd-P-C-C/H torsions for {biaryl Cy^1 Cy^2} follow this symmetry rule: $\{t_1\ t_2\ t_3\} = \{-t_2\ -t_1\ -t_3\}$. This gives rise to five different possible combinations for two cyclohexyl substituents (when following the same *anti*/*gauche*

classifications as outlined above); *aa*, ag^+, g^+a, g^+g^-, g^+g^+. The CyCy conformation populations for the available structures are as follows: *aa* (4) g^+a (16) g^+g^- (1).

DFT studies focusing on SPhos (and XPhos) have been carried out by Barder and Buchwald, studying both the oxidative addition step for PhCl,[24] and the amination of dimethylamine, ethylamine or aniline.[25a] In these studies, the authors identified five conformers for SPhos, by varying the Pd-P-C-C torsion when coordinated to [Pd(SPhos)(Ph)(Cl)]. Two of the lowest energy structures exhibited an η^1-interaction between the *ortho* carbon (crystallographically, an interaction between Pd···C_{ipso} is observed),[27] defined here as conformer $\mathbf{S_a}$. The remaining three conformers have the biphenyl ring under the ligand ($\mathbf{S_c}$), with the orientations of the two cyclohexyl groups influencing the overall conformer stability observed by Barder. Overall, the conformer distribution in work by Barder and Buchwald was as follows: *aa* (3) ag^+ (6) g^+a (1) g^+g^- (5), which differs from the crystallographically observed conformer populations. In addition, there is a structural difference between the g^+a conformer observed most commonly in the CSD, and the ag^+ conformer found by Barder and Buchwald; this is illustrated in Figure SI2g. It is likely that the thermodynamically more favourable conformer is seen in the crystal structures (g^+a), suggesting Barder and Buchwald's computational results have not identified the correct SPhos or XPhos conformers.

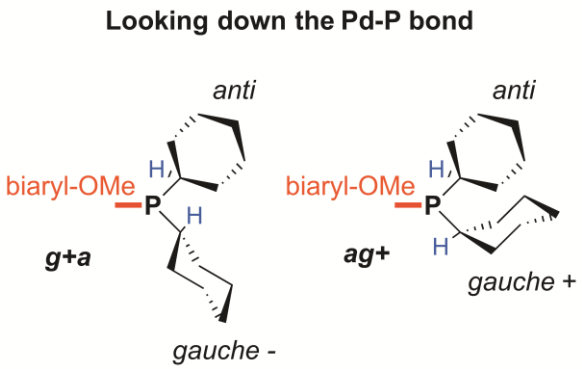

Figure SI2g Comparison of conformers; g^+a is the most common conformer with respect to the two cyclohexyl rings in SPhos, whereas ag^+ was studied extensively by Barder and Buchwald.[24-25]

With a view to exploring this further, conformers from crystal structures and those used in Barder & Buchwald's (B&B) computational work[24-25] were computed for the same catalytic intermediate, complex **5**, [Pd(SPhos)(Ph)(Br)] at the BP86/BSJ1 level in Jaguar (see section SI1a for details). Geometries from crystal structures were modified at the Pd metal centre, whilst B&B geometries were changed from *chloro* to *bromo* oxidative addition product species. Three distinct conformers were identified, as shown in Table SI2e. From the comparison of BEPLIS/LENWEH with B&B(16) for conformer $\mathbf{S_a}$ of SPhos, the energy difference for an incorrect CyCy conformation ($\boldsymbol{ag^+}$) can be estimated as ≈ 3 kcal mol^{-1}.

Table SI2e: Relative potential energies (B3LYP/BSJ1, in kcal mol^{-1}) and structural parameters (torsions in °; bond lengths in Å) from [Pd(SPhos)(Ph)(Br)] calculations, for different conformations of SPhos.

Structure	Rel. E.	Pd-P-C-C biaryl	Pd-P-C-H Cy^1		Pd-P-C-H Cy^2		CyCy	SPhos conf.	Pd···(X)
BEPLIS[a]	0.0	-4.3	-163.9	*a*	-65.5	g^-	$\boldsymbol{g^+a}$	$\mathbf{S_a}$	2.553 (C)
LENWEH[a]	0.0	-4.5	-163.1	*a*	-65.8	g^-	$\boldsymbol{g^+a}$	$\mathbf{S_a}$	2.554 (C)
B&B(16)	2.9	17.0	-69.2	g^-	174.3	*a*	$\mathbf{ag^+}$	$\mathbf{S_a}$	2.581 (C)
MAKBIK	3.8	-7.5	-166.9	*a*	-157.5	*a*	***aa***	$\mathbf{S_a}$	2.589 (C)
B&B(23)	4.2	59.4	-74.3	g^-	165.8	*a*	$\mathbf{ag^+}$	$\mathbf{S_b}$	2.311 (O)
B&B(21)	6.9	-78.9	-41.5	g^-	61.8	g^+	$\mathbf{g^+g^-}$	$\mathbf{S_b}$	2.371 (O)
JIMMEY[b]	7.2	63.1	-57.9	g^-	72.5	g^+	$\mathbf{g^+g^-}$	$\mathbf{S_b}$	3.214 (O)
B&B(20)[b]	7.2	-63.1	-72.5	g^-	57.9	g^+	$\mathbf{g^+g^-}$	$\mathbf{S_b}$	3.214 (O)
MAKBEG	10.0	155.7	-175.0	*a*	-63.9	g^-	$\boldsymbol{g^+a}$	$\mathbf{S_c}$	N/A
B&B(18)	10.7	151.7	-178.9	*a*	-150.7	*a*	***aa***	$\mathbf{S_c}$	N/A
GODREX[b]	11.3	-143.2	51.6	g^+	175.3	*a*	$\boldsymbol{g^+a}$	$\mathbf{S_c}$	N/A
JIMMIC[b]	11.3	143.2	-175.3	*a*	-51.6	g^-	$\boldsymbol{g^+a}$	$\mathbf{S_c}$	N/A

[a] structures are identical [b] structure is enantiomeric

We computed each of the three distinct conformers shown in Scheme SI2a, identified from crystal structures, for both the free ligand and when bound to palladium, with best method relative Gibbs energies given in Table SI2f. For the free ligand, conformer $\mathbf{S_a}$ has the lowest Gibbs energy, with $\mathbf{S_c}$ higher in Gibbs energy by 4.3 kcal mol^{-1}. Conformer $\mathbf{S_b}$ could not be optimized for the monoligated species [Pd(SPhos)] or the free ligand, suggesting that the Pd···O interaction observed in crystal structures is likely an artefact of an overcrowded palladium centre and solid-state crystal packing.

Table SI2f B3LYP-D2/BS2 Gibbs energies in kcal mol^{-1} for the oxidative addition of PhBr to $[Pd(SPhos)_n]$ for conformers $\mathbf{S_a}$ and $\mathbf{S_c}$ of SPhos

	$\Delta G°$ (90 °C) + ΔG_{solv}	$\mathbf{S_a}$	$\mathbf{S_c}$
	L = SPhos	0.0	4.3
$\mathbf{1_{SP}}$	[PdL]	12.1	2.4
$\mathbf{2_{SP}}$	$[PdL_2]$	0.3[a,b]	7.4[a,c]
$\mathbf{3_{SP}}$	[Pd(PhBr)L]	11.0	13.7
$\mathbf{4_{SP}}^{\ddagger}$	$[Pd(Ph^{\cdots}Br)L]^{\ddagger}$	19.6	24.0
$\mathbf{5_{SP}}$	[Pd(Ph)(Br)L]	-19.5	-9.4
$\mathbf{6_{SP}}^{\ddagger}$	$[Pd(PhBr)L_2]^{\ddagger}$	29.1	-

[a] Lowest energy conformer of $[Pd(SPhos)_2]$ is $\mathbf{S_{ab}}$, and the energies shown here are calculated relative to this complex.

[b] $\mathbf{S_{ac}}$; geometry taken from crystal structure *trans*-$[Pd(SPhos)_2]$, CSD ref. MAKBIK[16]

[c] $\mathbf{S_{cc}}$; geometry taken from crystal structure *trans*-[$PdCl_2(SPhos)_2$], CSD ref. MAKBEG[16]

The SPhos dimer discussed in the main paper, ***s*-10$_{SP}$**, was built directly from the *chloro*-dimer found in the CSD (ref. JIMMEY),[17] replacing Cl with Br and this showed the $\mathbf{S_b}$ conformer of SPhos. The Pd···O interactions observed for this *syn* dimer are likely an artefact of solid-state packing, which were retained after DFT optimization of the large structure in the gas phase, but conformational change is perhaps unlikely for optimisation of such a crowded complex.

The results shown in the main text are predominately for conformer $\mathbf{S_a}$, with the exception of **3$_{SP}$** ($\mathbf{S_c}$) and **10$_{SP}$** ($\mathbf{S_b}$). The bisligated PdL_2 complex, **2$_{SP}$** contains an $\mathbf{S_a}$ and $\mathbf{S_b}$ conformer, while the associative displacement transition state (**6$_{SP}$**‡) contains $\mathbf{S_a}$ and $\mathbf{S_c}$ for both the bromo and chloro aryl halide systems studied. Where ligand dissociation occurs, the most stable free ligand conformer of SPhos ($\mathbf{S_a}$) has been used to calculate relative energies.

SI3. Summary and Analysis of Available Experimental Kinetic Data

From our previous work[28]

k_{obs} = ((k_B × T) / h) × exp(-ΔG_{act} / RT)) **(Eq. 1)**

Rearrange Eq. 1 to form; ΔG_{act} = - RT × ln(k_{obs} × (h / (k_B × T))) **(Eq. 2)**

Where k_{obs} = experimentally observed rate constant, k_B = 1.38 × 10^{-23} J K^{-1} Boltzmann constant, T = temperature in K, h = 6.626 × 10^{-34} J s Planck constant, ΔG_{act} = free energy of activation in kcal mol^{-1}, and R = 0.00198 kcal K^{-1} mol^{-1} is the gas constant. Note that using Eq. 2 for bimolecular reactions where k_{obs} is in s^{-1} dm^3 mol^{-1} produces a free energy of activation that implicitly contains a reference to a standard state for the translational degrees of freedom of 1 mol dm^{-3}, so is consistent with the free energies as computed in this work.

Available experimental data:

a) PCy3

i) PdL_2 + L ⇌ PdL_3

Results reported by Mitchell and Baird:[29] In toluene, ΔH = 21 kJ mol^{-1}, ΔS = 59 J K^{-1} mol^{-1} for [$Pd(PCy_3)_2$] + PCy_3 from NMR data at between –68 and –85 °C. Extrapolation gives K_D = 0.3 at 25 °C and 1.5 at 100 °C, which can be used to estimate Δ*G*° of binding (=−RT ln K), giving –0.7 kcal mol^{-1} at 25 °C, and +0.3 kcal mol^{-1} at 100 °C.

NMR analysis reported by Barrios-Landeros *et al.*[30] suggests that at low temperatures (−60 to −80 °C), [$Pd(PCy_3)_3$] is the dominant species in the presence of more than 0.030 M added PCy_3, whereas at low concentration of added ligand, [$Pd(PCy_3)_2$] is the major species observed in solution at −80 °C.

ii) Oxidative addition of PhBr to PdL_n

Baird *et al.* investigated the kinetics of the oxidative addition of PhBr to [Pd(PCy3)2] in toluene-d_8 solution at 25 °C.[31] In the absence of additional ligand, the reaction was found to be first order in [$Pd(PCy_3)_2$], giving a pseudo-first order rate law, with an apparent rate constant given by *k*[PhBr] + *k*', with *k* = 1.3 × 10^{-3} M^{-1} s^{-1} and *k*' = 6.1 × 10^{-4} s^{-1}. Using **Eq. 2**, this gives $\Delta G^{‡}$= 21.3 and 21.7 kcal mol^{-1} respectively. They also determined k_{obs} as a function of [PhBr] in the presence of 1 equivalent of PCy_3, giving *k* = 1.6 × 10^{-3} s^{-1} at conditions similar to those used by Barrios-Landeros *et al.*[30] This corresponds to $\Delta G^{‡}$ =21.2 kcal mol^{-1}.

Barrios-Landeros *et al.* investigated this reaction in toluene at 10 °C (Fig. 12 in the paper),[30] considering [PhBr] = 0.95 – 7.6 M with [PCy_3] = 0.19 M. Reactivity is first-order with respect to [PhBr]. The line fitted in Fig. 12 of this study[30] corresponds to 1/k=−173 + 3590/[PhBr], with an intercept very

close to zero. Hence k_{app} = [PhBr] x 1/3590. They also considered [PCy_3] = 0.060M to 0.38 M with [PhBr] = 1.9 M. In this case, the fitted line corresponds to 1/k = 1370+2860*[L] due to PdL_2/PdL_3 equilibrium. k for reaction of PdL_2 is 1/1370 s^{-1}. Leaving aside the complication of the PdL_2/PdL_3 equilibrium, they find that Rate = k [Pd][PhBr] with k = 3×10^{-4} M^{-1} s^{-1}. $\Delta G^{\ddagger}$ = 21 kcal mol^{-1}.

A third study by Brown, Jutand *et al.*,[32] carried out in THF at 25 °C, rate dependence on [PCy_3] has not been considered and the authors report k = 0.025 M^{-1} s^{-1}. This rate is about twenty times larger than those reported by other groups as outlined above, which may be in part due to the difference in solvent used.

iii) Oxidative addition of PhCl to PdL_n

In this case, Barrios-Landeros *et al.* report data at 70 °C in toluene (Fig. 9 in the paper).[30] Dependence on L is now inverse with no intercept. Dependence on [PhCl] is linear, essentially no intercept, $1/k_{app}$ =13500 / [PhCl] s^{-1} for L = 0.01. Rate = k [Pd] [PhCl] / [L] = k_{app} [Pd] with k_{app} = [PhCl]/13500. So k/[L]=1/13500 hence k = 7.4×10^{-7} s^{-1}. $\Delta G^{\ddagger}$ = 29.4 kcal/mol.

Brown, Jutand *et al.*[32] report k = 0.015 M^{-1} s^{-1} at 25 °C in THF. Ligand concentration was not controlled and may be very low (1% of 2mM). $k_{app} = k$ / [PCy_3] is thus likely to be ill-defined and much larger than k. Comparing with Barrios-Landeros *et al.*[30], and assuming no T-dependence, this would imply that $[L]_{free} \approx 7.4 \times 10^{-7}$ / 0.015 or 5×10^{-5} M.

b) PPh_3

i) $PdL_2 + L \rightleftharpoons PdL_3$

In solution, ligand dissociation to the [PdL_3] species **11_{Ph}** is known to be near quantitative except at very low temperatures and in the presence of excess phosphine.[33] Dissociation of **11_{Ph}** to form bisligated **2_{Ph}** is found experimentally to be unfavourable, with a dissociation equilibrium constant of the order of 10^{-4} M.[34]

ii) Oxidative addition of PhBr to PdL_n

For reaction with [$Pd(PPh_3)_4$], an apparent rate constant k_{app} = 9×10^{-4} M^{-1} s^{-1} was measured at 25 °C in THF.[32] Under the conditions used, [$Pd(PPh_3)_4$] will have fully dissociated to [$Pd(PPh_3)_3$], which will itself be in equilibrium with a small amount of [$Pd(PPh_3)_2$]. Assuming that the latter reacts with PhBr with a rate constant k, then [$Pd(PPh_3)_3$] will decay with $k_{app} = kK/[PPh_3]$. Given that [PPh_3] was equal to 0.002 M in the experiments, this means that kK equals 1.8×10^{-6} s^{-1}, equivalent to an activation Gibbs energy of 25.2 kcal mol^{-1}.

iii) Oxidative addition of PhCl to PdL_n

The study by Brown, Jutand *et al.*[32] reports this ligand/substrate combination as unreactive in both THF and DMF.

c) P^tBu_3

Data relevant to this ligand[30] have been analysed in our previous work and details may be found in the ESI there.[28] In summary, analysis of results for oxidative addition of PhBr to $[Pd(P^tBu_2Ad)_2]$ at 90 °C in toluene give ΔG_{act} = 27.4 kcal mol^{-1}. For the oxidative addition of PhCl to $[Pd(P^tBu_2Cy)_2]$ at 100 °C in toluene, ΔG_{act} = 29.3 kcal mol^{-1}.

SI4. Details of additional calculations

a. PhX coordination isomers

Limited space in our previous study[28] restricted us from being able to comment and discuss our investigation of isomers of intermediates $\mathbf{3}_{tBu}$ and $\mathbf{5}_{tBu}$ for each phenyl halide substrate (PhI, PhBr and PhCl). The calculated "best method" energies for these species are shown in Table SI4a.

Table SI4a Relative Gibbs energies ($\Delta G°$ (90 °C) + ΔG_{solv}) respectively for PhI, PhBr and PhCl) in kcal mol^{-1} for the oxidative addition of PhX to $[Pd(P^tBu_3)_2]$ for isomers of intermediates **3** and **5**.

	$\Delta G°$ (90 °C) + ΔG_{solv}		**PhI**	**PhBr**	**PhCl**
$\mathbf{3}_{tBu}$	[Pd(PhX)L]	η^2-*meta-para*	21.2	18.6	21.8
$\mathbf{3}_{tBu}$	[Pd(PhX)L]	η^2-*ortho-meta*	17.4	19.0	22.0
$\mathbf{3}_{tBu}$	[Pd(PhX)L]	η^2-*ipso-ortho*	[b]	20.0	24.2
$\mathbf{3}_{tBu}$	[Pd(PhX)L]	ipso	15.8	21.1	24.3
$\mathbf{3}_{tBu}$	[Pd(PhX)L]	via X	23.6	23.0	29.4
$\mathbf{3}_{tBu}^{‡}$	[Pd(PhX)L]‡	*meta*	[a]	19.8	[a]
$\mathbf{3}_{tBu}^{‡}$	[Pd(PhX)L]‡	*ortho*	[a]	21.8	[a]
$\mathbf{3}_{tBu}^{‡}$	[Pd(PhX)L]‡	*ipso*	[a]	22.0	[a]
$\mathbf{5}_{tBu}$	[Pd(Ph)(X)L]	*trans* halide	-3.1	-1.2	4.1
$\mathbf{5}_{tBu}$	[Pd(Ph)(X)L]	*trans* VS	[b]	[b]	7.2
$\mathbf{5}_{tBu}$	[Pd(Ph)(X)L]	*trans* aryl	6.3	12.5	20.1
$\mathbf{5}_{tBu}^{‡}$	[Pd(Ph)(X)L]‡	"Y"	12.3	11.8	25.3

[a] not calculated for this conformer

[b] would not optimise for this isomer

For the coordinated substrate ($\mathbf{3}_{tBu}$), low barriers to rotation of the phenyl ring relative to the metal fragment were found (Fig. SI4a), with a preference for η^2-binding to the Pd centre. The *mp* isomer was found to be lowest in relative free energy for both the PhBr and PhCl substrates. However, unusually for the *iodo* congener the lowest free energy isomer of **3** has the Pd atom bound to the C_{ipso} atom of the PhI substrate. Transition states between these isomers were computed for the *bromo* system, and were found to give low barriers, between 1.2- 2.0 kcal mol^{-1}, supporting the hypothesis that isomerisation from the lowest free energy isomer (η^2-mp) to the isomer required for monoligated oxidative addition to occur (*ipso*) is a low energy process.

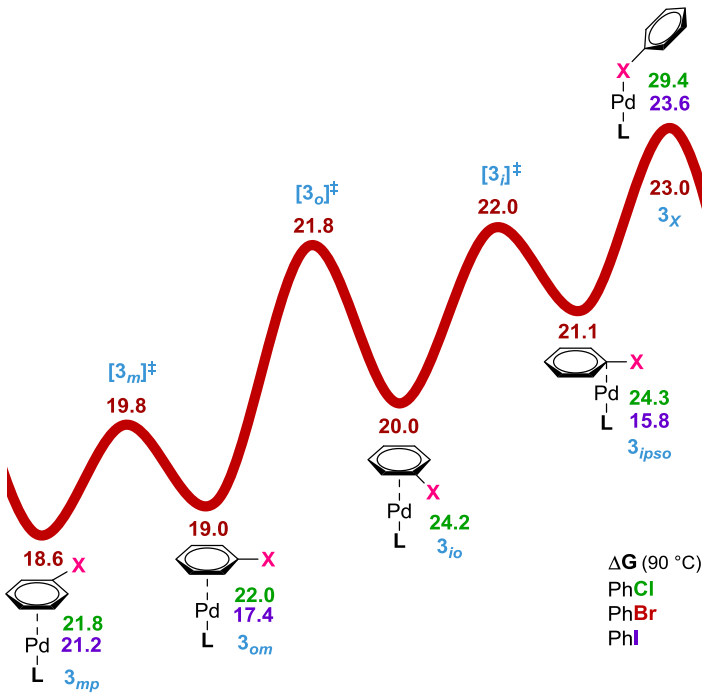

Figure SI4a: Lowest energy isomer and free energy profile ($\Delta G°$ (90 °C) + ΔG_{solv}) for isomers of $\mathbf{3_{tBu}}$, including isomerisation transition states. All data relative to $\mathbf{2_{tBu}}$ [Pd(P^tBu_3)$_2$].

The oxidative addition product ($\mathbf{5_{tBu}}$) has three possible "T"-shaped isomers (Fig. SI4b). Due to the strong *trans*-influence of the phenyl ligand, the ligand is most likely to be *trans* to the halide in **5**.[35] This agrees with known *trans* influences and is consistent with crystal structures observed in the CSD. The *trans* vacant site (VS) isomer was only successfully optimised for the *chloro* system. The Y-shaped isomerisation transition state for $\mathbf{5_{tBu}}$, $\mathbf{5_{tBu}}^‡$, confirms that interconversion between the isomers of **5** is less likely for PhBr and PhCl, and that the *trans* halide isomer will be preferentially formed over the other isomer species.

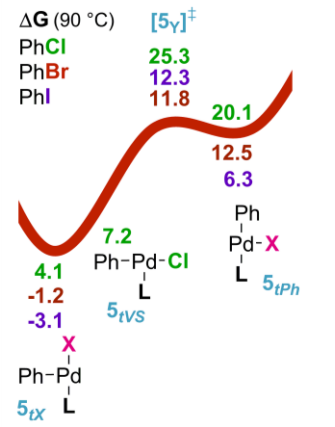

Figure SI4b: Lowest energy isomer and free energy profile ($\Delta G°$ (90 °C) + ΔG_{solv}) for isomers of $\mathbf{5_{tBu}}$, including isomerisation transition states. All data relative to $\mathbf{2_{tBu}}$ [Pd(P^tBu_3)$_2$].

b. DFT-D geometry and potential energy (BS1) effects on favoured palladium coordination number

Table SI4 b L = PCy_3, all energies are potential energies and given in units of kcal mol^{-1}, distances in Å.

Complex	ΔE (B3LYP/BS1)	Pd-P (B3LYP)	ΔE-D(BS1) at B3LYP geom.	ΔE(BP86/BS1)	Pd-P (BP86)	ΔE-D (opt. w. B3LYP-D2/BS1)	Pd-P (B3LYP-D2)
[PdL]	34.6 (38.6)[a]	2.229 (2.236)[a]	43.4 (46.1)[a]	42.4	2.197	47.3	2.211
[PdL_2]	0.0	2.342, 2.327 (2.326, 2.327)[a]	0.0	0.0	2.301, 2.303	0.00	2.283, 2.289
[PdL_3]	7.1 (7.2)[a]	2.431, 2.435, 2.467 (2.435, 2.432, 2.467)[a]	-26.3 (-29.1)[a]	3.0	2.395, 2.391, 2.418	-35.86	2.328, 2.323, 2.348

[a]Results shown in parentheses used a different starting geometry, but are consistent with that used for optimisation at other levels of theory shown.

Table SI4c L = PPh_3, all energies are potential energies and given in units of kcal mol^{-1}, distances in Å.

Complex	ΔE (B3LYP/BS1)	Pd-P (B3LYP)	ΔE-D(BS1) at B3LYP geom.	ΔE(BP86/BS1)	Pd-P (BP86)	ΔE-D (opt. w. B3LYP-D2/BS1)	Pd-P (B3LYP-D2)
[PdL]	34.5	2.215	40.1	38.9	2.178	43.4	2.194
[PdL_2]	0.0	2.308, 2.309	0.0	0.0	2.284, 2.285	0.0	2.280, 2.279
[PdL_3]	-6.8	2.372, 2.375, 2.377	-30.8	not converged		-39.3	2.306, 2.305, 2.317
[PdL_4]	-1.0	2.534, 2.534, 2.535, 2.536	-35.5			-76.1	2.410, 2.410, 2.412, 2.407

Table SI4d L = SPhos, all energies are potential energies and given in units of kcal mol^{-1}, distances in Å.

Complex	ΔE (B3LYP/BS1)	Pd-P (B3LYP)	ΔE-D(BS1) at B3LYP geom.	ΔE(BP86/BS1)	Pd-P (BP86)	ΔE-D (opt. w. B3LYP-D2/BS1)	Pd-P (B3LYP-D2)
[PdL]	15.7	2.293	33.5	21.3	2.269	53.5	2.256
[PdL_2]	0.0	2.323, 2.337	0.0	0.0	2.310, 2.298	0.0	2.280, 2.285

c. DFT-D geometry and energy (ΔE, ΔG) effects on transition state preference for oxidative addition of PhCl to [$Pd(PCy_3)_2$] (Path A *vs.* C)

Table SI4e, kcal mol^{-1}

Complex	ΔE, B3LYP/BS1	ΔE, B3LYP-D2/BS1	$\Delta G°$ (90 °C), B3LYP/BS1	$\Delta G°$ (90 °C), B3LYP-D2/BS1	ΔE, B3LYP-D2/BS1//B3LYP/BS1
PdL_2 + PhCl	0.00	0.00	0.00	0.00	0.00
Path A, $[4]^‡$	30.35	32.46	29.14	30.85	35.87
Path C, $[6]^‡$	26.45	0.51	46.17	19.03	4.36

d. Effect of dispersion correction on potential energies for PCy_3

Table SI4f, all structures optimised with B3LYP/BS1, relative energies in kcal mol^{-1} (see section SI1a for computational details)[19]

a) PhBr	Δ*E*, B3LYP-D2/BS1	Δ*E*, B3LYP-D3/BS1	Δ*E*, B3LYP-D3-BJ/BS1
1	45.04	44.18	46.20
2	0.00	0.00	0.00
3	20.34	21.90	21.46
[4]‡	28.12	27.53	26.78
5	0.72	1.67	0.63
[6]‡	6.96	7.84	7.16
[8]‡	-2.53	-1.49	-3.84
t-9	-50.92	-47.99	-51.44
a-10	-20.43	-19.64	-21.78
11	-29.44	-27.33	-28.53

b) PhCl	Δ*E*, B3LYP-D2/BS1	Δ*E*, B3LYP-D3/BS1	Δ*E*, B3LYP-D3-BJ/BS1
1	45.04	44.18	46.20
2	0.00	0.00	0.00
3	20.42	21.98	21.55
[4]‡	36.27	35.63	35.03
5	4.77	5.90	4.35
[6]‡	7.59	8.86	8.10
[8]‡	4.36	5.18	2.70
11	-29.44	-27.33	-28.53

e. Results for L=PH_3

The different oxidative addition pathways have also been computed for **L** = PH_3 with PhBr (Table S14g) and PhCl (Table S14h). These results are not discussed in the manuscript but are included here.

Table Sl4g: PhBr/PH_3

		ΔE	ΔE	ΔG (90°C)	ΔG (90°C) + ΔG_{solv}	ΔE	ΔG (90°C)	ΔG (90°C) + ΔG_{solv}
		B3LYP /BS1	B3LYP /BS2	B3LYP /BS2	B3LYP /BS2	B3LYP-D2 /BS2	B3LYP-D2 /BS2	B3LYP-D2 /BS2
1_H	[Pd(**PH_3**)] + **PH_3** + PhBr	30.2	30.0	20.0	17.3	31.3	21.3	18.7
2_H	[Pd(**PH_3**)$_2$] + PhBr	0.0	0.0	0.0	0.0	0.0	0.0	0.0
3_H	[Pd(**PH_3**)(PhBr)] + **PH_3**	12.0	13.5	11.1	13.0	8.9	6.5	8.4
$4_H^‡$	[Pd(**PH_3**)(Ph···Br)]‡ + **PH_3**	20.3	20.9	19.4	21.4	18.1	16.6	18.6
5_H	[Pd(**PH_3**)(Ph)(Br)] + **PH_3**	2.1	1.2	0.3	-0.8	-2.6	-3.4	−4.5
$6_H^‡$	[Pd(**PH_3**)$_2$(PhBr)]‡	12.1	13.3	18.6	20.9	5.3	10.6	12.9
7_H	[Pd(**PH_3**)$_2$(PhBr)]	-1.5	-1.0	1.3	5.0	-3.9	-1.5	2.2
$8_H^‡$	[Pd(**PH_3**)$_2$(Ph···Br)]‡	14.4	15.2	24.5	25.3	8.1	17.3	18.1
c-**9_H**	[Pd(**PH_3**)$_2$(Ph)(Br)] (*cis)*	-15.6	-16.6	-4.9	-7.7	-24.1	-12.5	−15.2
t-**9_H**	[Pd(**PH_3**)$_2$(Ph)(Br)] (*trans*)	-21.3	-24.5	-9.8	-11.9	-28.9	-17.2	−19.3
a-**10_H**	½[(μ-Br)$_2$Pd$_2$(**PH_3**)$_2$(Ph)$_2$] + **PH_3** (*anti*)	-15.0	-15.7	-7.6	-6.2	-23.3	-15.2	−13.8
s-**10_H**	½[(μ-Br)$_2$Pd$_2$(**PH_3**)$_2$(Ph)$_2$] + **PH_3** (*syn*)	-15.1	-15.8	-9.6	-8.1	-23.4	-17.2	−15.7
11_H	[Pd(**PH_3**)$_3$] – **PH_3** + PhBr	-10.1	-9.6	0.1	-0.7	-11.9	-2.3	−3.1
12_H	[Pd(**PH_3**)$_4$] – 2**PH_3** + PhBr	-17.4	-17.1	3.0	0.2	-23.1	-3.0	−5.8

Table SI4h: $PhCl/PH_3$

		ΔE	ΔE	ΔG (100°C)	ΔG (100°C) + ΔG_{solv}	ΔE	ΔG (100°C)	ΔG (100°C) + ΔG_{solv}
		B3LYP /BS1	B3LYP /BS2	B3LYP /BS2	B3LYP /BS2	B3LYP-D2 /BS2	B3LYP-D2 /BS2	B3LYP-D2 /BS2
$\mathbf{1_H}$	[Pd($\mathbf{PH_3}$)] + $\mathbf{PH_3}$ + PhCl	30.2	30.0	19.8	17.1	31.3	21.1	18.5
$\mathbf{2_H}$	[Pd($\mathbf{PH_3}$)$_2$] + PhCl	0.0	0.0	0.0	0.0	0.0	0.0	0.0
$\mathbf{3_H}$	[Pd($\mathbf{PH_3}$)(PhCl)] + $\mathbf{PH_3}$	12.0	13.5	11.5	13.0	8.9	7.0	8.5
$\mathbf{4_H}^{‡}$	[Pd($\mathbf{PH_3}$)(Ph···Cl)]‡ + $\mathbf{PH_3}$	28.1	27.5	25.3	26.5	24.9	22.7	23.9
$\mathbf{5_H}$	[Pd($\mathbf{PH_3}$)(Ph)(Cl)] + $\mathbf{PH_3}$	6.2	3.5	2.3	0.4	-0.3	-1.4	-3.4
$\mathbf{6_H}^{‡}$	[Pd($\mathbf{PH_3}$)$_2$(PhCl)]‡	12.1	13.1	19.5	21.6	5.3	11.7	13.7
$\mathbf{7_H}$	[Pd($\mathbf{PH_3}$)$_2$(PhCl)]	2.1	3.7	9.6	10.2	-4.2	1.7	2.3
$\mathbf{8_H}^{‡}$	[Pd($\mathbf{PH_3}$)$_2$(Ph···Cl)]‡	20.9	20.5	30.7	30.9	13.7	23.9	24.1
c-$\mathbf{9_H}$	[Pd($\mathbf{PH_3}$)$_2$(Ph)(Cl)] (*cis)*	-15.5	-14.1	2.2	3.1	-21.3	-5.0	-4.1
t-$\mathbf{9_H}$	[Pd($\mathbf{PH_3}$)$_2$(Ph)(Cl)] (*trans*)	-16.8	-19.2	-8.0	-10.8	-26.4	-15.3	-18.0
a-$\mathbf{10_H}$	½[(μ-Cl)$_2$Pd$_2$($\mathbf{PH_3}$)$_2$(Ph)$_2$] + $\mathbf{PH_3}$ (*anti*)	-12.2	-14.4	-7.7	-7.0	-21.5	-14.8	-14.1
s-$\mathbf{10_H}$	½[(μ-Cl)$_2$Pd$_2$($\mathbf{PH_3}$)$_2$(Ph)$_2$] + $\mathbf{PH_3}$ (*syn*)	-12.2	-14.4	-8.3	-7.4	-21.5	-15.4	-14.6
$\mathbf{11_H}$	[Pd($\mathbf{PH_3}$)$_3$] – $\mathbf{PH_3}$ + PhCl	-10.1	-9.6	0.3	-0.5	-11.9	-2.0	-2.9
$\mathbf{12_H}$	[Pd($\mathbf{PH_3}$)$_4$] – 2$\mathbf{PH_3}$ + PhCl	-17.4	-17.1	3.4	0.6	-23.1	-2.6	-5.4

SI5. Solvent Coordination to [PdP^{t}Bu$_3$]

Toluene isomers of **3$_{tBu}$** and the associative displacement transition state (**6$_{tBu}^{‡}$**) have also been computed and are discussed here. The role of solvent in a palladium-catalyzed cross-coupling reaction was explicitly modeled by Green and co-workers for an NHC catalyst in a benzene solution.[23a] The monoligated species (**1**) was stabilized by the η^2-coordination of an arene, when the arene is either the solvent (in this case benzene) or the reacting aryl halide. Solvent association was shown to be less favourable for bulkier ligands. More recently, solvent coordination also been considered with P-donor ligands. [23b-d]

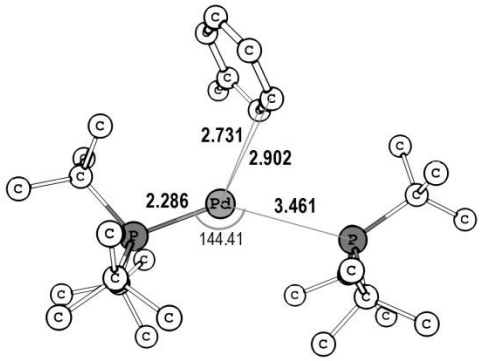

Figure SI5a– Optimized geometry of ^{tol}**6$_{tBu}^{‡}$**. Relevant bond **lengths** (Å) and *angles* (°) are shown. Hydrogen atoms omitted for clarity.

An associative displacement transition state for toluene and the bulky P^{t}Bu$_3$ catalyst was optimized (^{tol}**6$_{tBu}^{‡}$**, Figure SI5a), as well as isomers of the monophosphine solvated [Pd(L)(toluene)] complex (^{tol}**3$_{tBu}$**). The isomers (see Scheme SI5a) have been defined by the coordination of the palladium atom to the toluene substrate occurring either via η^2-binding to π-bonds between *p* - *para*, *m* - *meta*, *o* - *ortho* or *i* - *ipso* carbons of toluene, or by coordinating only at the *ipso* carbon.

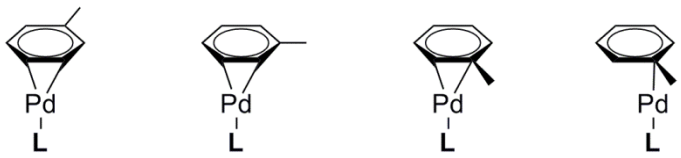

(η^2-*mp*)-^{tol}**3$_{tBu}$** (η^2-*om*)-^{tol}**3$_{tBu}$** (η^2-*io*)-^{tol}**3$_{tBu}$** (*ipso*)-^{tol}**3$_{tBu}$**

Scheme SI5a – Isomer conformations of ^{tol}**3$_{tBu}$**; [Pd(P^{t}Bu$_3$)(toluene)]

Table SI5a – B3LYP-D2/BS2 Gibbs energies in kcal mol^{-1} for isomers of [Pd(P^{t}Bu$_3$)(toluene)] (^{tol}**3$_{tBu}$**) and a related associative displacement transition state (^{tol}**6$_{tBu}$**‡).

	$\Delta G°$ (70 °C) + ΔG_{solv}	P^{t}Bu$_3$
2$_{tBu}$	[Pd(**P^{t}Bu$_3$**)$_2$]	0.0
^{tol}**6$_{tBu}$**‡	[Pd(**P^{t}Bu$_3$**)$_2$(toluene)]‡	29.2
(η^2-*mp*)-^{tol}3$_{tBu}$	[Pd(**P^{t}Bu$_3$**)(toluene)]	20.9
(η^2-o*m*)-^{tol}3$_{tBu}$	[Pd(**P^{t}Bu$_3$**)(toluene)]	20.7
(η^2-*io*)-^{tol}3$_{tBu}$	[Pd(**P^{t}Bu$_3$**)(toluene)]	19.2
(*ipso*)-^{tol}3$_{tBu}$	[Pd(**P^{t}Bu$_3$**)(toluene)]	20.7
^{PhCl}**6$_{tBu}$**‡	[Pd(**P^{t}Bu$_3$**)$_2$(PhCl)]‡	27.6
(η^2-*mp*)-^{PhCl}**3$_{tBu}$**	[Pd(**P^{t}Bu$_3$**)(PhCl)]	19.2
(η^2-*io*)-^{PhCl}**3$_{tBu}$**	[Pd(**P^{t}Bu$_3$**)(PhCl)]	21.6
^{PhBr}**6$_{tBu}$**‡	[Pd(**P^{t}Bu$_3$**)$_2$(PhBr)]‡	28.6
(η^2-*mp*)-^{PhBr}**3$_{tBu}$**	[Pd(**P^{t}Bu$_3$**)(PhBr)]	20.1
(η^2-*io*)-^{PhBr}**3$_{tBu}$**	[Pd(**P^{t}Bu$_3$**)(PhBr)]	21.5
^{PhI}**6$_{tBu}$**‡	[Pd(**P^{t}Bu$_3$**)$_2$(PhI)]‡	33.3
(η^2-*mp*)-^{PhI}**3$_{tBu}$**	[Pd(**P^{t}Bu$_3$**)(PhI)]	19.6
(η^2-*io*)-^{PhI}**3$_{tBu}$**	[Pd(**P^{t}Bu$_3$**)(PhI)]	-

The calculated Gibbs energies given in Table SI5a show an interesting trend when compared to values for the corresponding geometries with aryl halides (PhX = PhCl, PhBr and PhI) calculated in our earlier work.[28] Firstly, for the toluene adduct (^{tol}**3$_{tBu}$**) the lowest energy isomer is (η^2-*io*) with the palladium atom coordinating to the π-system between the *ipso* and *ortho* carbon atoms, whilst for all aryl halide adducts (^{PhX}**3$_{tBu}$**) the *meta-para* isomer (η^2-*mp*) was lower in energy. Gibbs energies at 70 °C for the monophosphine aryl adduct, **3**, show the following trend with respect to phenyl substituent: Cl = Me < I < Br . Comparison of the associative displacement transition state (**6$_{tBu}$**‡) shows a similar trend, *i.e.* Cl < Br < Me < I.

The barriers to associative displacement imply that toluene solvent molecules will compete with phenyl bromide and iodide substrates to coordinate to the palladium metal centre, suggesting that toluene adduct formation might consume too much of the palladium catalyst at high reaction temperatures. However, the barrier is lower for phenyl chloride substrates, as might be expected since monophosphine oxidative addition has been identified as rate limiting in this case..

The direct formation of **3** from **1**, as part of the dissociative pathway (Path A), has been shown to be unlikely, as coordination of a solvent molecule, instead of the desired halide substrate, is a viable and likely alternative as solvent will be present in excess. Even with a bulky, electron-donating phosphine

to support a monoligated [Pd(L)] species (**1**) such as P^tBu_3, it is unlikely that the 12 electron complex would be a persistent intermediate in solution. On the other hand, the relatively weakly-bound solvent adducts would be in equilibrium with small amounts of **1**, which can then, ultimately, undergo coordination by substrate to yield **3**. This is not experimentally readily distinguished from direct coordination of aryl halide to **1**. Formation of **3** could also proceed via concerted displacement pathways from the solvate species.

Table SI2b: Breakdown of energies for toluene coordination to the [Pd($PtBu_3$)$_2$] catalyst.

		ΔE	ΔE	ΔG (90°C)	ΔG (90°C) + ΔG_{solv}	ΔE	ΔG (90°C)	ΔG (90°C) + ΔG_{solv}
		B3LYP /BS1	B3LYP /BS2	B3LYP /BS2	B3LYP /BS2	B3LYP-D2 /BS2	B3LYP-D2 /BS2	B3LYP-D2 /BS2
2_{tBu}	[Pd($PtBu_3$)$_2$] + PhBr + toluene	0.0	0.0	0.0	0.0	0.0	0.0	0.0
(η^2-*mp*)-^{tol}**3_{tBu}**	[Pd(**P^tBu_3**)(toluene)]	15.8	15.8	16.1	14.4	22.3	22.5	20.9
(η^2-o*m*)-^{tol}**3_{tBu}**	[Pd(**P^tBu_3**)(toluene)]	15.8	15.8	15.6	14.2	22.3	22.1	20.7
(η^2-*io*)-^{tol}**3_{tBu}**	[Pd(**P^tBu_3**)(toluene)]	17.5	17.3	16.0	13.7	22.7	21.4	19.1
(*ipso*)-^{tol}**3_{tBu}**	[Pd(**P^tBu_3**)(toluene)]	17.4	17.2	17.4	15.4	22.6	22.8	20.8
^{tol}**6_{tBu}**‡	[Pd(**P^tBu_3**)$_2$(toluene)]‡	25.4	27.1	39.3	39.7	17.2	29.4	29.8
$^{tol/PhBr}$**6_{tBu}**‡	[Pd(**P^tBu_3**)(PhBr)(toluene)]‡	23.1	25.4	36.9	36.4	19.1	30.7	30.1

Table S1: Breakdown of energies for $[Pd(PCy_3)_n]$ at different reaction temperatures.

a) 90 °C

		Δ***E***	Δ***E***	Δ***G*** **(90°C)**	Δ***G*** **(90°C) +** ΔG_{solv}	Δ***E***	Δ***G*** **(90°C)**	Δ***G*** **(90°C) +** ΔG_{solv}
		B3LYP /BS1	B3LYP /BS2	B3LYP /BS2	B3LYP /BS2	B3LYP-D2 /BS2	B3LYP-D2 /BS2	B3LYP-D2 /BS2
$\mathbf{1_{Cy}}$	[Pd(**PCy_3**)] + **PCy_3** + PhBr	34.6	32.9	20.1	8.1	43.4	30.6	18.5
$\mathbf{2_{Cy}}$	[Pd(**PCy_3**)$_2$] + PhBr	0.0	0.0	0.0	0.0	0.0	0.0	0.0
$\mathbf{11_{Cy}}$	[Pd(**PCy_3**)$_3$] – **PCy_3** + PhBr	7.1	10.3	32.3	39.3	-26.3	-4.2	2.7

b) 10 °C

		Δ***E***	Δ***E***	Δ***G*** **(10°C)**	Δ***G*** **(10°C) +** ΔG_{solv}	Δ***E***	Δ***G*** **(10°C)**	Δ***G*** **(10°C) +** ΔG_{solv}
		B3LYP /BS1	B3LYP /BS2	B3LYP /BS2	B3LYP /BS2	B3LYP-D2 /BS2	B3LYP-D2 /BS2	B3LYP-D2 /BS2
$\mathbf{1_{Cy}}$	[Pd(**PCy_3**)] + **PCy_3** + PhBr	34.6	32.9	22.5	10.5	43.4	32.9	20.9
$\mathbf{2_{Cy}}$	[Pd(**PCy_3**)$_2$] + PhBr	0.0	0.0	0.0	0.0	0.0	0.0	0.0
$\mathbf{11_{Cy}}$	[Pd(**PCy_3**)$_3$] – **PCy_3** + PhBr	7.1	10.3	28.1	35.0	-26.3	-8.5	-1.5

c) -60 °C

		Δ***E***	Δ***E***	Δ***G*** **(-60°C)**	Δ***G*** **(-60°C) +** ΔG_{solv}	Δ***E***	Δ***G*** **(-60°C)**	Δ***G*** **(-60°C) +** ΔG_{solv}
		B3LYP /BS1	B3LYP /BS2	B3LYP /BS2	B3LYP /BS2	B3LYP-D2 /BS2	B3LYP-D2 /BS2	B3LYP-D2 /BS2
$\mathbf{1_{Cy}}$	[Pd(**PCy_3**)] + **PCy_3** + PhBr	34.6	32.9	25.1	13.0	43.4	35.5	23.5
$\mathbf{2_{Cy}}$	[Pd(**PCy_3**)$_2$] + PhBr	0.0	0.0	0.0	0.0	0.0	0.0	0.0
$\mathbf{11_{Cy}}$	[Pd(**PCy_3**)$_3$] – **PCy_3** + PhBr	7.1	10.3	23.9	30.8	-26.3	-12.7	-5.8

Table S2: Relative energies at all levels of theory for oxidative addition of PhBr to [Pd(PCy_3)$_2$]. a) 90°C

		Δ*E*	**Δ*E***	**Δ*G* (90°C)**	**Δ*G* (90°C) + ΔG_{solv}**	**Δ*E***	**Δ*G* (90°C)**	**Δ*G* (90°C) + ΔG_{solv}**
		B3LYP /BS1	B3LYP /BS2	B3LYP /BS2	B3LYP /BS2	B3LYP-D2 /BS2	B3LYP-D2 /BS2	B3LYP-D2 /BS2
1_{Cy}	[Pd(**PCy_3**)] + **PCy_3** + PhBr	34.6	32.9	20.1	8.1	43.4	30.6	18.5
2_{Cy}	[Pd(**PCy_3**)$_2$] + PhBr	0.0	0.0	0.0	0.0	0.0	0.0	0.0
3_{Cy}	[Pd(**PCy_3**)(PhBr)] + **PCy_3**	16.8	16.9	14.9	10.5	20.4	18.4	14.0
$4_{Cy}^{‡}$	[Pd(**PCy_3**)(Ph···Br)]‡ + **PCy_3**	23.0	22.7	21.5	17.6	27.8	26.6	22.7
5_{Cy}	[Pd(**PCy_3**)(Ph)(Br)] + **PCy_3**	1.2	-0.2	-0.5	-9.2	-0.3	-0.7	-9.3
$6_{Cy}^{‡}$	[Pd(**PCy_3**)$_2$(PhBr)]‡	20.4	21.5	34.6	42.0	8.1	21.2	28.6
$8_{Cy}^{‡}$	[Pd(**PCy_3**)$_2$(Ph···Br)]‡	21.0	23.3	40.6	44.1	-0.2	17.1	20.6
***t*-9_{Cy}**	[Pd(**PCy_3**)$_2$(Ph)(Br)] (*trans*)	-23.2	-21.0	-0.2	0.4	-48.7	-27.9	-27.3
***a*-10_{Cy}**	½[(μ-Br)$_2$Pd$_2$(**PCy_3**)$_2$(Ph)$_2$] + **PCy_3** (*anti*)	-11.7	-12.3	-1.9	-5.3	-21.1	-10.6	-14.1
11_{Cy}	[Pd(**PCy_3**)$_3$] – **PCy_3** + PhBr	7.1	10.3	32.3	39.3	-26.3	-4.2	2.7

b) 10°C

		ΔE	*ΔE*	*ΔG* (10°C)	*ΔG* (10°C) + ΔG_{solv}	*ΔE*	*ΔG* (10°C)	*ΔG* (10°C) + ΔG_{solv}
		B3LYP /BS1	B3LYP /BS2	B3LYP /BS2	B3LYP /BS2	B3LYP-D /BS2	B3LYP-D /BS2	B3LYP-D /BS2
1_{Cy}	[Pd(**PCy_3**)] + **PCy_3** + PhBr	34.6	32.9	22.5	10.5	43.4	32.9	20.9
2_{Cy}	[Pd(**PCy_3**)$_2$] + PhBr	0.0	0.0	0.0	0.0	0.0	0.0	0.0
3_{Cy}	[Pd(**PCy_3**)(PhBr)] + **PCy_3**	16.8	16.9	20.9	16.5	20.4	24.4	20.0
$4_{Cy}^{‡}$	[Pd(**PCy_3**)(Ph···Br)]‡ + **PCy_3**	23.0	22.7	27.2	23.3	27.8	32.3	28.4
5_{Cy}	[Pd(**PCy_3**)(Ph)(Br)] + **PCy_3**	1.2	-0.2	5.1	-3.5	-0.3	5.0	-3.6
$6_{Cy}^{‡}$	[Pd(**PCy_3**)$_2$(PhBr)]‡	20.4	21.5	38.2	45.6	8.1	24.8	32.2
$8_{Cy}^{‡}$	[Pd(**PCy_3**)$_2$(Ph···Br)]‡	21.0	23.3	42.8	46.3	-0.2	19.3	22.8
t-9_{Cy}	[Pd(**PCy_3**)$_2$(Ph)(Br)] (*trans*)	-23.2	-21.0	1.4	2.1	-48.7	-26.2	-25.6
a-10_{Cy}	½[(μ-Br)$_2$Pd$_2$(**PCy_3**)$_2$(Ph)$_2$] + **PCy_3** (*anti*)	-11.7	-12.3	1.9	-1.6	-21.1	-6.9	-10.4
11_{Cy}	[Pd(**PCy_3**)$_3$] – **PCy_3** + PhBr	7.1	10.3	28.1	35.0	-26.3	-8.5	-1.5

Table S3: Relative energies at all levels of theory for oxidative addition of PhBr to [Pd(PPh$_3$)$_2$].

		ΔE	ΔE	ΔG (90°C)	ΔG (90°C) + ΔG_{solv}	ΔE	ΔG (90°C)	ΔG (90°C) + ΔG_{solv}
		B3LYP /BS1	B3LYP /BS2	B3LYP /BS2	B3LYP /BS2	B3LYP-D2 /BS2	B3LYP-D2 /BS2	B3LYP-D2 /BS2
1$_{Ph}$	[Pd(**PPh$_3$**)] + **PPh$_3$** + PhBr	34.5	31.5	19.8	9.8	40.1	28.4	18.4
2$_{Ph}$	[Pd(**PPh$_3$**)$_2$] + PhBr	0.0	0.0	0.0	0.0	0.0	0.0	0.0
3$_{Ph}$	[Pd(**PPh$_3$**)(PhBr)] + **PPh$_3$**	16.4	15.6	15.7	12.6	17.4	17.5	14.4
4$_{Ph}^{‡}$	[Pd(**PPh$_3$**)(Ph···Br)]‡ + **PPh$_3$**	23.2	22.0	23.9	21.1	25.5	27.5	24.7
5$_{Ph}$	[Pd(**PPh$_3$**)(Ph)(Br)] + **PPh$_3$**	1.6	-0.3	0.3	-5.5	-1.3	-0.7	-6.4
6$_{Ph}^{‡}$	[Pd(**PPh$_3$**)$_2$(PhBr)]‡	16.7	17.3	30.6	37.8	4.4	17.7	24.9
8$_{Ph}^{‡}$	[Pd(**PPh$_3$**)$_2$(Ph···Br)]‡	17.0	18.5	33.1	39.9	0.3	15.0	21.8
***c*-9$_{Ph}$**	[Pd(**PPh$_3$**)$_2$(Ph)(Br)] (*cis*)	-9.9	-8.4	10.4	11.5	-33.7	-14.8	-13.7
***t*-9$_{Ph}$**	[Pd(**PPh$_3$**)$_2$(Ph)(Br)] (*trans*)	-18.8	-17.0	1.8	3.0	-39.7	-21.0	-19.8
***a*-10$_{Ph}$**	½[(μ-Br)$_2$Pd$_2$(**PPh$_3$**)$_2$(Ph)$_2$] + **PPh$_3$** (*anti*)	-11.4	-12.8	-4.4	-5.1	-20.8	-12.5	-13.2
11$_{Ph}$	[Pd(**PPh$_3$**)$_3$] – **PCy$_3$** + PhBr	-6.8	-4.6	13.2	24.4	-30.8	-13.1	-1.9
12$_{Ph}$	[Pd(**PPh$_3$**)$_3$] – 2**PPh$_3$** + PhBr	-1.0	4.6	44.9	63.9	-35.8	4.6	23.5

Table S4: Relative energies at all levels of theory for oxidative addition of PhBr to [Pd(SPhos)$_2$].

For the lowest energy free ligand conformer **S$_a$**

			Δ***E***	Δ***E***	Δ***G*** **(90°C)**	Δ***G*** **(90°C) + ΔG_{solv}**	Δ***E***	Δ***G*** **(90°C)**	Δ***G*** **(90°C) + ΔG_{solv}**
			B3LYP /BS1	B3LYP /BS2	B3LYP /BS2	B3LYP /BS2	B3LYP-D2 /BS2	B3LYP-D2 /BS2	B3LYP-D2 /BS2
^{a}**1$_{SP}$**	[Pd(^{a}**SPhos**)] + ^{a}**SPhos** + PhBr		21.9	18.7	3.9	-9.1	39.9	25.0	12.1
^{c}**1$_{SP}$**	[Pd(^{c}**SPhos**)] + ^{a}**SPhos** + PhBr		38.1	26.6	4.1	-19.4	48.4	25.9	2.4
^{ac}**2$_{SP}$**	[Pd(^{ac}**SPhos**)$_2$] + PhBr		-2.0	-2.5	-2.1	-2.0	-0.2	0.2	0.3
^{ab}**2$_{SP}$**	[Pd(^{ab}**SPhos**)$_2$] + PhBr		0.0	0.0	0.0	0.0	0.0	0.0	0.0
^{cc}**2$_{SP}$**	[Pd(^{cc}**SPhos**)$_2$] + PhBr		2.8	2.1	4.1	1.3	8.2	10.2	7.4
^{a}**3$_{SP}$**	[Pd(^{a}**SPhos**)(PhBr)] + ^{a}**SPhos**		6.9	5.6	3.3	-2.2	18.8	16.4	11.0
^{c}**3$_{SP}$**	[Pd(^{c}**SPhos**)(PhBr)] + ^{a}**SPhos**		11.7	10.3	6.4	-1.1	25.1	21.1	13.7
^{a}**4$_{SP}$**‡	[Pd(^{a}**SPhos**)(Ph···Br)]‡ + ^{a}**SPhos**		13.8	12.4	9.4	4.8	27.2	24.1	19.6
^{c}**4$_{SP}$**‡	[Pd(^{c}**SPhos**)(Ph···Br)]‡ + ^{a}**SPhos**		18.5	16.8	15.4	7.6	33.2	31.8	24.0
^{a}**5$_{SP}$**	[Pd(^{a}**SPhos**)(Ph)(Br)] + ^{a}**SPhos**		-13.1	-14.5	-16.1	-26.9	-7.1	-8.7	-19.5
^{c}**5$_{SP}$**	[Pd(^{c}**SPhos**)(Ph)(Br)] + ^{a}**SPhos**		-4.5	-6.6	-8.3	-19.8	3.8	2.1	-9.4
^{ac}**6$_{SP}$**‡	[Pd(^{ac}**SPhos**)$_2$(PhBr)]‡		24.2	26.1	39.7	42.4	12.7	26.4	29.1
s-10$_{SP}$	½[(μ-Br)$_2$Pd$_2$(^{bb}**SPhos**)$_2$(Ph)$_2$] + **SPhos** (*syn*)	+	-18.7	-19.5	-11.4	-15.6	-23.8	-15.7	-19.9

Table S5: Relative energies at all levels of theory for oxidative addition of PhBr to [Pd($PtBu_3$)$_2$].

		ΔE	ΔE	ΔG (90°C)	ΔG (90°C) + ΔG_{solv}	ΔE	ΔG (90°C)	ΔG (90°C) + ΔG_{solv}
		B3LYP /BS1	B3LYP /BS2	B3LYP /BS2	B3LYP /BS2	B3LYP -D2 /BS2	B3LYP -D2 /BS2	B3LYP -D2 /BS2
1_{tBu}	[Pd(**P^tBu_3**)] + **P^tBu_3** + PhBr	33.5	31.5	19.7	11.6	45.6	33.8	25.7
2_{tBu}	[Pd(**P^tBu_3**)$_2$] + PhBr	0.0	0.0	0.0	0.0	0.0	0.0	0.0
3_{tBu}	[Pd(**P^tBu_3**)(PhBr)] + **P^tBu_3**	15.6	15.3	14.5	13.0	22.3	20.1	18.6
$4_{tBu}^{‡}$	[Pd(**P^tBu_3**)(Ph···Br)]‡ + **P^tBu_3**	21.5	21.0	21.1	19.8	29.5	28.2	26.9
5_{tBu}	[Pd(**P^tBu_3**)(Ph)(Br)] + **P^tBu_3** (*trans halide*)	2.2	1.4	2.4	-4.2	5.7	5.4	-1.2
5_{tBu}	[Pd(**P^tBu_3**)(Ph)(Br)] + **P^tBu_3** (*trans aryl*)	11.3	10.7	8.9	5.3	19.3	16.1	12.5
$5_{tBu}^{‡}$	[Pd(**P^tBu_3**)(Ph)(Br)] + **P^tBu_3** (*isomerization TS*)	14.0	13.3	5.8	3.2	23.3	14.4	11.8
$6_{tBu}^{‡}$	[Pd(**P^tBu_3**)$_2$(PhBr)]‡	25.3	26.9	39.2	39.8	16.2	28.6	29.2
***t*-9_{tBu}**	[Pd(**P^tBu_3**)$_2$(Ph)(Br)] (*trans*)	14.4	16.2	33.7	29.5	-3.3	14.2	10.0
***a*-10_{tBu}**	½[(μ-Br)$_2$Pd$_2$(**P^tBu_3**)$_2$(Ph)$_2$] + **P^tBu_3** (*anti*)	-1.0	-1.9	8.0	5.2	-4.5	4.1	1.3
***s*-10_{tBu}**	½[(μ-Br)$_2$Pd$_2$(**P^tBu_3**)$_2$(Ph)$_2$] + **P^tBu_3** (*syn*)	-0.9	-1.8	8.2	5.1	-4.4	4.1	1.0

Table S6: Overview of computational methodologies used in related work on complexes with PCy_3, PPh_3, SPhos and $PtBu_3$ ligands. (SP – single point correction, GO – geometry optimisation)

Ligand	DFT method for energies reported	Gibbs energies	Gibbs energy of solvation	Dispersion	Reference
PCy_3	B3LYP/DZP+ & HF/DZP ONIOM	✓	x	x	36
PPh_3	B3LYP, B3LYP-D, M06/TZP+	✓	✓(SP)	✓ (SP)	37
	B3LYP/DZP	✓	✓(SP)	x	38
	PBE0-D3/TZP	✓	✓(SP)	✓ (GO)	39
	B3PW91/DZP	✓	✓(SP)	x	40
	B3LYP/TZP+	✓	✓(SP)	x	41
	B3LYP/DZP in QM/MM	x	x	x	20
	PBE-D, AIMD with QM/MM		explicit solvent	✓	23d
	M06/DZP	✓	x	✓	42
SPhos	B3LYP/DZP	✓	x	x	24
	PBE0-D3/TZP	✓	✓(SP)	✓ (GO)	43
$PtBu_3$	B3LYP-D2/TZP+	✓	✓(SP)	✓(SP)	28
	B3LYP/TZP+	x	some (SP)	x	35
	PBE0-D3/TZP	✓	✓(SP)	✓ (GO)	39
	B3LYP/DZP+	✓	x	x	36
	PBE/PBE/DZP+	✓	✓(SP)	x	44
	B3PW91/DZP	✓	✓(SP)	x	40
	B3LYP/TZP+	✓	✓(SP)	x	41
	PBE/DZP	x	✓(GO)	x	45
	B3LYP, B3PW91, BLYP, M06L, M052X/DZP+	✓	✓(GO)	M06L & M052X	23b,c
	B3LYP/DZP	x	✓(GO)	x	46

Table S7: Relative energies at all levels of theory for oxidative addition of PhCl to $[Pd(PCy_3)_2]$.

		ΔE	ΔE	ΔG (90°C)	ΔG (90°C) + ΔG_{solv}	ΔE	ΔG (90°C)	ΔG (90°C) + ΔG_{solv}
		B3LYP /BS1	B3LYP /BS2	B3LYP /BS2	B3LYP /BS2	B3LYP-D2 /BS2	B3LYP-D2 /BS2	B3LYP-D2 /BS2
1_{Cy}	[Pd(**PCy_3**)] + **PCy_3** + PhCl	34.6	32.9	20.1	8.1	43.4	30.6	18.5
2_{Cy}	[Pd(**PCy_3**)$_2$] + PhCl	0.0	0.0	0.0	0.0	0.0	0.0	0.0
3_{Cy}	[Pd(**PCy_3**)(PhCl)] + **PCy_3**	16.9	16.8	15.7	11.1	20.3	19.2	14.6
$4_{Cy}^{‡}$	[Pd(**PCy_3**)(Ph···Cl)]‡ + **PCy_3**	30.4	30.5	29.3	25.6	36.0	34.8	31.1
5_{Cy}	[Pd(**PCy_3**)(Ph)(Cl)] + **PCy_3**	4.8	1.8	1.9	-6.9	1.7	1.9	-7.0
$6_{Cy}^{‡}$	[Pd(**PCy_3**)$_2$(PhCl)]‡	20.6	21.5	34.1	40.5	8.5	21.0	27.5
$8_{Cy}^{‡}$	[Pd(**PCy_3**)$_2$(Ph···Cl)]‡	26.5	27.2	44.5	45.9	5.1	22.4	23.8
***t*-9_{Cy}**	[Pd(**PCy_3**)$_2$(Ph)(Cl)] (*trans*)	-24.5	-25.0	-7.4	-7.9	-51.3	-33.7	-34.2
***a*-10_{Cy}**	½[(μ-Cl)$_2$Pd$_2$(**PCy_3**)$_2$(Ph)$_2$] + **PCy_3** (*anti*)	-9.8	-12.3	-1.8	-5.5	-19.8	-9.4	-13.0
11_{Cy}	[Pd(**PCy_3**)$_3$] – **PCy_3** + PhCl	7.1	10.3	32.3	39.3	-26.3	-4.2	2.7

Table S8: Relative energies at all levels of theory for oxidative addition of PhCl to $[Pd(PPh_3)_2]$.

			ΔE	ΔE	ΔG (90°C)	ΔG (90°C) + ΔG_{solv}	ΔE	ΔG (90°C)	ΔG (90°C) + ΔG_{solv}
			B3LYP /BS1	B3LYP /BS2	B3LYP /BS2	B3LYP /BS2	B3LYP-D2 /BS2	B3LYP-D2 /BS2	B3LYP-D2 /BS2
1_{Ph}	[Pd(**PPh_3**)] + **PPh_3** + PhCl		34.5	31.5	19.8	9.8	40.1	28.4	18.4
2_{Ph}	[Pd(**PPh_3**)$_2$] + PhCl		0.0	0.0	0.0	0.0	0.0	0.0	0.0
3_{Ph}	[Pd(**PPh_3**)(PhCl)] + **PPh_3**		16.5	15.4	16.0	12.4	17.3	18.0	14.4
$4_{Ph}^{‡}$	[Pd(**PPh_3**)(Ph···Cl)]‡ + **PPh_3**		30.6	28.1	26.8	23.0	32.1	30.7	26.9
5_{Ph}	[Pd(**PPh_3**)(Ph)(Cl)] + **PPh_3**		5.7	1.7	1.8	-5.4	0.8	0.9	-6.4
$6_{Ph}^{‡}$	[Pd(**PPh_3**)$_2$(PhCl)]‡		16.7	16.8	28.9	36.4	5.0	17.1	24.6
$8_{Ph}^{‡}$	[Pd(**PPh_3**)$_2$(Ph···Cl)]‡		23.5	23.5	38.5	43.6	4.6	19.6	24.7
***c*-9_{Ph}**	[Pd(**PPh_3**)$_2$(Ph)(Cl)] (*cis*)		-6.6	-7.5	11.2	10.2	-31.5	-12.8	-13.8
***t*-9_{Ph}**	[Pd(**PPh_3**)$_2$(Ph)(Cl)] (*trans*)		-16.3	-17.3	1.4	2.4	-38.2	-19.6	-18.5
***a*-10_{Ph}**	½[(μ-Cl)$_2$Pd$_2$(**PPh_3**)$_2$(Ph)$_2$] + **PPh_3** (*anti*)	+	-8.7	-12.2	-3.7	-5.0	-19.3	-10.7	-12.1
11_{Ph}	[Pd(**PPh_3**)$_3$] – **PCy_3** + PhCl		-6.8	-4.6	13.2	24.4	-30.8	-13.1	-1.9
12_{Ph}	[Pd(**PPh_3**)$_3$] – 2**PPh_3** + PhCl		-1.0	4.6	42.5	61.4	-35.8	2.2	21.1

Table S9: Relative energies at all levels of theory for oxidative addition of PhCl to [Pd(SPhos)].

For the lowest energy free ligand conformer $\mathbf{S_a}$

		ΔE	ΔE	ΔG (90°C)	ΔG (90°C) + ΔG_{solv}	ΔE	ΔG (90°C)	ΔG (90°C) + ΔG_{solv}
		B3LYP /BS1	B3LYP /BS2	B3LYP /BS2	B3LYP /BS2	B3LYP-D2 /BS2	B3LYP-D2 /BS2	B3LYP-D2 /BS2
$^{a}\mathbf{1}_{SP}$	[Pd(^{a}**SPhos**)] + ^{a}**SPhos** + PhCl	21.9	18.7	3.9	-9.1	39.9	25.0	12.1
$^{c}\mathbf{1}_{SP}$	[Pd(^{c}**SPhos**)] + ^{a}**SPhos** + PhCl	38.1	26.6	4.1	-19.4	48.4	25.9	2.4
$^{ac}\mathbf{2}_{SP}$	[Pd(^{ac}**SPhos**)$_2$] + PhCl	-2.0	-2.5	-2.1	-2.0	-0.2	0.2	0.3
$^{ab}\mathbf{2}_{SP}$	[Pd(^{ab}**SPhos**)$_2$] + PhCl	0.0	0.0	0.0	0.0	0.0	0.0	0.0
$^{cc}\mathbf{2}_{SP}$	[Pd(^{cc}**SPhos**)$_2$] + PhCl	2.8	2.1	4.1	1.3	8.2	10.2	7.4
$^{a}\mathbf{3}_{SP}$	[Pd(^{a}**SPhos**)(PhCl)] + ^{a}**SPhos**	7.0	5.4	0.7	-5.1	19.0	14.3	8.5
$^{a}\mathbf{4}_{SP}^{‡}$	[Pd(^{a}**SPhos**)(Ph···Cl)]‡ + ^{a}**SPhos** (*trans halide*)	21.5	18.4	13.9	9.6	31.8	27.3	23.0
$^{a}\mathbf{4}_{SP}^{‡}$	[Pd(^{a}**SPhos**)(Ph···Cl)]‡ + ^{a}**SPhos** (*trans aryl*)	20.7	18.1	14.8	7.8	32.6	29.3	22.3
$^{a}\mathbf{5}_{SP}$	[Pd(^{a}**SPhos**)(Ph)(Cl)] + ^{a}**SPhos**	-9.6	-13.5	-14.4	-25.9	-5.3	-6.2	-17.7
$^{ac}\mathbf{6}_{SP}^{‡}$	[Pd(^{ac}**SPhos**)$_2$(PhCl)]‡	23.8	25.2	40.6	42.1	12.1	27.4	29.0
$\mathbf{s\text{-}10}_{SP}$	½[(μ-Cl)$_2$Pd$_2$(^{bb}**SPhos**)$_2$(Ph)$_2$] + **SPhos** (*syn*)	-16.7	-19.4	-10.3	-15.8	-24.5	-15.4	-20.9

Table S10: Relative energies at all levels of theory for oxidative addition of PhCl to [Pd(PtBu$_3$)$_2$].

		Δ***E***	Δ***E***	Δ***G*** **(90°C)**	Δ***G*** **(90°C) + ΔG_{solv}**	Δ***E***	Δ***G*** **(90°C)**	Δ***G*** **(90°C) + ΔG_{solv}**
		B3LYP /BS1	B3LYP /BS2	B3LYP /BS2	B3LYP /BS2	B3LYP -D2 /BS2	B3LYP -D2 /BS2	B3LYP -D2 /BS2
1$_{tBu}$	[Pd(**P^{t}Bu$_3$**)] + **P^{t}Bu$_3$** + PhCl	33.5	31.5	19.7	11.6	45.6	33.8	25.7
2$_{tBu}$	[Pd(**P^{t}Bu$_3$**)$_2$] + PhCl	0.0	0.0	0.0	0.0	0.0	0.0	0.0
3$_{tBu}$	[Pd(**P^{t}Bu$_3$**)(PhCl)] + **P^{t}Bu$_3$**	15.7	15.2	13.8	12.2	22.1	23.3	21.8
4$_{tBu}^{‡}$	[Pd(**P^{t}Bu$_3$**)(Ph···Cl)]‡ + **P^{t}Bu$_3$**	30.2	27.9	27.1	23.6	35.0	36.9	33.3
5$_{tBu}$	[Pd(**P^{t}Bu$_3$**)(Ph)(Cl)] + **P^{t}Bu$_3$** (*trans halide*)	6.4	3.4	4.4	-3.1	8.0	11.6	4.1
6$_{tBu}^{‡}$	[Pd(**P^{t}Bu$_3$**)$_2$(PhCl)]‡	24.8	26.1	39.8	39.0	16.2	32.5	31.7
***t*-9$_{tBu}$**	[Pd(**P^{t}Bu$_3$**)$_2$(Ph)(Cl)] (*trans*)	11.8	11.1	29.5	24.3	-7.7	13.4	8.1
***a*-10$_{tBu}$**	½[(μ-Cl)$_2$Pd$_2$(**P^{t}Bu$_3$**)$_2$(Ph)$_2$] + **P^{t}Bu$_3$** (*anti*)	0.1	-2.6	7.3	4.4	-4.5	8.1	5.1

References

1. a) A. D. Becke, *Phys. Rev. A*, 1988, **38**, 3098-3100; b) A. D. Becke, *J. Chem. Phys.*, 1993, **98**, 5648-5652; c) C. T. Lee, W. T. Yang and R. G. Parr, *Phys. Rev. B*, 1988, **37**, 785-789; d) S. H. Vosko, L. Wilk and M. Nusair, *Can. J. Phys.*, 1980, **58**, 1200-1211; e) B. Miehlich, A. Savin, H. Stoll and H. Preuss, *Chem. Phys. Lett.*, 1989, **157**, 200-206; f) J. C. Slater, *Quantum Theory of Molecules and Solids, Vol. 4: The Self-Consistent Field for Molecules and Solids*, McGraw-Hill, New York, 1974.
2. a) P. C. Hariharan and J. A. Pople, *Theor. Chem. Acc.*, 1973, **28**, 213-222; b) M. J. Frisch, J. A. Pople and J. S. Binkley, *J. Chem. Phys.*, 1984, **80**, 3265-3269.
3. A. Bergner, M. Dolg, W. Kuechle, H. Stoll and H. Preuss, *Mol. Phys.*, 1993, **80**, 1431.
4. K. A. Peterson, D. Figgen, M. Dolg and H. Stoll, *J. Chem. Phys.*, 2007, **126**, 124101.
5. a) B. Marten, K. Kim, C. Cortis, R. A. Friesner, R. B. Murphy, M. N. Ringnalda, D. Sitkoff and B. Honig, *J. Phys. Chem.*, 1996, **100**, 11775; b) D. J. Tannor, B. Marten, R. B. Murphy, R. A. Friesner, D. Sitkoff, A. Nicholls, M. N. Ringnalda, W. A. Goddard III and B. Honig, *J. Am. Chem. Soc.*, 1994, **116**, 11875.
6. a) K. A. Peterson, D. Figgen, E. Goll, H. Stoll and M. Dolg, *J. Chem. Phys.*, 2003, **119**, 11113-11123; b) K. A. Peterson, B. C. Shepler, D. Figgen and H. Stoll, *J. Phys. Chem.*, 2006, **110**, 13877-13883.
7. M. J. Frisch, J. A. Pople and J. S. Binkley, *J. Chem. Phys.*, 1984, **80**, 3265.
8. C. J. Cramer, *Faraday Discuss.*, 2010, **145**, 523-556.
9. a) S. Grimme, *J. Comput. Chem.*, 2004, **25**, 1463-1473; b) S. Grimme, *J. Comput. Chem.*, 2006, **27**, 1787-1799.
10. ORCA, An Ab Initio, DFT, and Semiempirical Electronic Structure Package Version 2.6.35, F. Neese, Universität Bonn, Germany, , 2007.
11. Jaguar 6.0, Schrödinger LLC, New York, NY, 2005.
12. P. J. Stephens, F. G. Devlin, C. F. Chabalowski and M. J. Frisch, *J. Phys. Chem.*, 1994`, **98**, 11623.
13. F. Allen, *Acta Cryst. B*, 2002, **58**, 380-388.
14. V. G. Andrianov, I. S. Akhrem, N. M. Chistovalova and Y. T. Struchkov, *Zh. Strukt. Khim.*, 1976, **17**, 135.
15. PCModel 9.0, Serena Software, Bloomington IN, USA, 2004.
16. T. E. Barder, S. D. Walker, J. R. Martinelli and S. L. Buchwald, *J. Am. Chem. Soc.*, 2005, **127**, 4685-4696.
17. M. R. Biscoe, T. E. Barder and S. L. Buchwald, *Angew. Chem. Int. Ed.*, 2007, **46**, 7232.
18. J. P. Perdew, *Phys. Rev. B*, 1986, **33**, 8822-8824.
19. a) S. Grimme, J. Antony, S. Ehrlich and H. Krieg, *J. Chem. Phys.*, 2010, **132**, 154104; b) S. Grimme, S. Ehrlich and L. Goerigk, *J. Comput. Chem.*, 2011, **32**, 1456-1465.
20. M. Besora, A. A. C. Braga, G. Ujaque, F. Maseras and A. Lledos, *Theor. Chem. Acc.*, 2010.
21. a) A. G. Orpen, *Acta Cryst. B*, 2002, **58**, 398; b) D. D. Ellis, M. F. Haddow, A. G. Orpen and P. J. Watson, *Dalton Trans.*, 2009, 10436-10445.
22. H. B. Buergi and J. D. Dunitz, *Acta Cryst. B*, 1988, **44**, 445.
23. a) J. C. Green, B. J. Herbert and R. Lonsdale, *J. Organomet. Chem.*, 2005, **690**, 6054-6067; b) E. Lyngvi and F. Schoenebeck, *Tetrahedron*, 2013, **69**, 5715-5718; c) F. Proutiere and F. Schoenebeck, *Angew. Chem. Int. Ed.*, 2011, **50**, 8192-8195; d) P. Vidossich, G. Ujaque and A. Lledos, *Chem. Commun.*, 2014, **50**, 661-663.
24. T. E. Barder, M. R. Biscoe and S. L. Buchwald, *Organometallics*, 2007, **26**, 2183-2192.
25. a) T. E. Barder and S. L. Buchwald, *J. Am. Chem. Soc.*, 2007, **129**, 12003-12010; b) R. Martin and S. L. Buchwald, *Acc. Chem. Res.*, 2008, **41**, 1461-1473.
26. F. H. Allen, *Acta Cryst. B*, 2002, **58**, 380.
27. S. D. Walker, T. E. Barder, J. R. Martinelli and S. L. Buchwald, *Angew. Chem. Int. Ed.*, 2004, **43**, 1871-1876.
28. C. L. McMullin, J. Jover, J. N. Harvey and N. Fey, *Dalton Trans.*, 2010, **39**, 10833-10836.
29. E. A. Mitchell and M. C. Baird, *Organometallics*, 2007, **26**, 5230-5238.
30. F. Barrios-Landeros, B. P. Carrow and J. F. Hartwig, *J. Am. Chem. Soc.*, 2009, **131**, 8141-8154.
31. E. A. Mitchell, P. G. Jessop and M. C. Baird, *Organometallics*, 2009, **28**, 6732-6738.

32. A. Kurbangalieva, D. Carmichael, K. K. M. Hii, A. Jutand and J. M. Brown, *Chem. Eur. J.*, 2014, **20**, 1116-1125.
33. a) B. E. Mann and A. Musco, *J. Chem. Soc. Dalton Trans.*, 1975, 1673-1677; b) J.-F. Fauvarque, F. Pflüger and M. Troupel, *J. Organomet. Chem.*, 1981, **208**, 419-427.
34. C. Amatore and F. Pfluger, *Organometallics*, 1990, **9**, 2276-2282.
35. C. L. McMullin, B. Rühle, M. Besora, A. G. Orpen, J. N. Harvey and N. Fey, *J. Mol. Cat. A*, 2010, **324**, 39-47.
36. F. Schoenebeck and K. N. Houk, *J. Am. Chem. Soc.*, 2010, **132**, 2496-2497.
37. M. S. G. Ahlquist and P.-O. Norrby, *Angew. Chem. Int. Ed.*, 2011, **50**, 11794-11797.
38. M. Ahlquist, P. Fristrup, D. Tanner and P.-O. Norrby, *Organometallics*, 2006, **25**, 2066-2073.
39. S. Kozuch and J. M. L. Martin, *ACS Catal.*, 2011, **1**, 246-253.
40. S. Moncho, G. Ujaque, A. Lledos and P. Espinet, *Chem. Eur. J.*, 2008, **14**, 8986-8994.
41. A. Ariafard and B. F. Yates, *J. Am. Chem. Soc.*, 2009, **131**, 13981-13991.
42. K. Vikse, T. Naka, J. S. McIndoe, M. Besora and F. Maseras, *ChemCatChem*, 2013, **5**, 3604-3609.
43. S. Kozuch and J. M. L. Martin, *Chem. Commun.*, 2011, **47**, 4935-4937.
44. Z. Li, Y. Fu, Q.-X. Guo and L. Liu, *Organometallics*, 2008, **27**, 4043-4049.
45. W.-J. Sun, W. Chu, L.-J. Yu and C.-F. Jiang, *Chin. J. Chem. Phys.*, 2010, **23**, 175-179.
46. M. Ahlquist and P.-O. Norrby, *Organometallics*, 2007, **26**, 550-553.